The role of serpentinization and magmatism in the formation of decoupling interfaces at magma-poor rifted margins

Morgane Gillard, Julie Tugend, Othmar Müntener, Gianreto Manatschal, Garry D. Karner, Julia Autin, Daniel Sauter, Patricio H Figueredo, Marc Ulrich

The role of serpentinization and magmatism in the formation of decoupling interfaces at magma-poor rifted margins

Morgane Gillard*[a1], Julie Tugend[a,b,c], Othmar Müntener[d], Gianreto Manatschal[a], Garry D. Karner[e] , Julia Autin[a], Daniel Sauter[a], Patricio H. Figueredo[e] , Marc Ulrich[a]

*Corresponding author: Morgane Gillard (morgane.gillard@upmc.fr)

(a) Institut de Physique du Globe de Strasbourg, UMR7516, Université de Strasbourg/EOST, CNRS, 1 rue Blessig, Strasbourg, Cedex, F-67084, France
(b) Sorbonne Université, CNRS-INSU, Institut des Sciences de la Terre Paris, ISTeP UMR 7193, F-75005 Paris, France
(c) Total SA, R&D department CSTJF, Pau, France
(d) Institute of Earth Sciences, University of Lausanne, Géopolis, CH-1015 Lausanne, Switzerland.
(e) ExxonMobil Upstream Integrated Solutions Company, Global Tectonics & Structure, 22777 Springwoods Village Parkway, Spring, Texas, USA
(1) Present address: Sorbonne Université, CNRS-INSU, Institut des Sciences de la Terre Paris, ISTeP UMR 7193, F-75005 Paris, France

Declarations of interest: none

Abstract

In spite of recent progress in the understanding of magma-poor rifted margins, the processes leading to the formation and evolution of the exhumed mantle domain and its transition toward steady state oceanic crust remain debated. In particular, the parameters controlling the progressive localization of extensional deformation and magmatic processes leading to the formation of an oceanic spreading center are poorly understood. In this paper, we highlight the occurrence of two major decoupling horizons controlling the structural and magmatic evolution of distal magma-poor rifted margins. They are marked by strong seismic reflectors located at about 1 sec TWTT (Upper Reflectors–UR) and 2 sec TWTT (Lower Reflectors–LR) below top basement in domains of exhumed mantle at several magma-poor rifted margins. Both reflection seismic observations and studies on the physical properties of serpentinized mantle suggest that the UR likely results from deformation localized along a rheological interface at about 3 km below top basement, associated with an abrupt change in the mechanical behavior of peridotites once they are serpentinized to ~15%. We suggest that this interface played a major role in successive fault re-organizations during formation of the exhumed mantle domain. The comparison of reflection seismic observations with Alpine field analogues suggests that the LR likely results from an interaction between magmatism, deformation and hydration reactions during final rifting. Based on our results, we suggest that during final rifting the strain distribution is controlled first by hydration and then by magmatic processes in the domain of exhumed mantle.

Keywords: Serpentinization; Magma-poor margins; Decoupling; Seismic interpretation

1. Introduction and scientific context

Major progress has been made in understanding the architecture of magma-poor rifted margins (e.g., Peron-Pinvidic et al., 2013; Reston, 2009). At present, it is generally accepted that the transition zone located between the edge of continental and first unambiguous oceanic crusts, also referred to as the Ocean Continent Transition (OCT), can include a zone of exhumed subcontinental serpentinized mantle. The presence of such a basement type is attested at several distal rifted margins based on drilling (e.g. Iberia-Newfoundland (Boillot et al., 1988; Sawyer et al., 1994; Whitmarsh et al., 1998; Tucholke et al., 2004); Tyrrhenian Sea (Bonatti et al., 1990)) and dredges (e.g. Australia-Antarctica (Beslier et al., 2004)). This is further supported by reflection and refraction seismic data (e.g. southern North Atlantic margins (Reston, 2007; Minshull, 2009)), or potential field data (e.g. SE-India (Nemcok et al., 2013); Bay of Biscay (Thinon et al., 2003; Tugend et al., 2014)). However, how this zone of exhumed mantle forms and evolves to steady state oceanic spreading remains an open question, notably, how extensional deformation interacts with serpentinization and onset of magmatic activity.

Evidence for polyphase deformation and an interaction with serpentinization and magmatic processes is inferred both from field observations and reflection seismic data (Desmurs et al., 2001, 2002; Picazo et al., 2016; Gillard et al., 2015). The organization and geometry of fault systems in exhumed mantle domains appear polyphase, showing in-sequence and/or out-of-sequence stepping of faults resulting in a complex final basement architecture (Reston and McDermott, 2011; Gillard et al., 2016a). However, the processes that control the stepping and evolution of these faults remain poorly constrained, as are the way high-angle normal faults interact with extensional detachment systems (exhumation faults) and the nature and depth of their decoupling levels (Boillot and Froitzheim, 2001; Reston and McDermott, 2011; Gillard et al., 2016b). On reflection seismic sections, normal faults often seem to interact with intra-basement decoupling interfaces that generally appear as strong reflections. A well-studied example is the S-reflector, located at the base of hyperextended continental crust of the Galicia rifted margin (Sibuet, 1992; Reston, 1996; Whitmarsh et al., 1996; Reston and Pérez-Gussinyé, 2007; Reston, 2009; Lymer et al. 2019). The S-reflector is commonly interpreted as a decollement due to the presence of a sole of serpentinized mantle, suggesting that hydration processes can control the structural evolution of hyperextended and exhumed mantle domains (Pérez-Gussinyé and Reston, 2001; Pérez-Gussinyé et al., 2001; Bayrakci et al., 2016). Other intra-basement reflectors have also been identified in more distal domains of magma-poor rifted margins, for example the Z reflection at the Newfoundland margin (Hopper et al., 2006) or the D reflection at the Labrador margins (Chian et al., 1995), which are localized in domains of exhumed mantle. In these newly formed domains, both serpentinization and magmatism control the composition, thermal state and rheology of the basement. Consequently, the nature and origin of these intra-basement reflections and the evolution and localization of deformation in these ultra-distal domains remain unclear.

The aim of this study is twofold. First, we describe different types of coherent seismic reflectors that may have acted as decoupling interfaces in exhumed mantle domains, using several examples of magma-poor rifted margins (Fig. 1). We describe their geometry, position and their geometrical relationship to fault structures. In a second part, we discuss the potential mechanisms related to their formation based on a multi-disciplinary approach and we explore the influence of hydrothermal circulation, serpentinization and magmatism on the structural evolution of ultra-distal domains at magma-poor rifted margins.

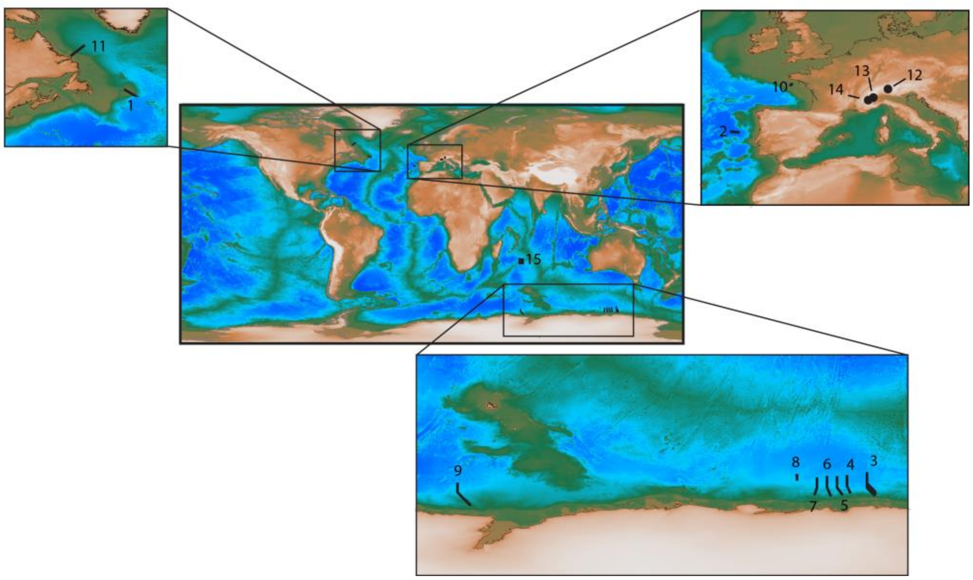

Figure 1: Location map of the different seismic profiles and field analogues described in this study. 1: Screech1 (Newfoundland margin); 2: IAM9 (Iberian margin); 3: GA228-27 (Antarctica margin); 4: GA228-25 (Antarctica margin); 5: GA228-24 (Antarctica margin); 6: GA228-23 (Antarctica margin); 7: GA228-22 (Antarctica margin); 8: GA229-10 (Antarctica margin); 9: GA228-06 (Antarctica margin); 10: Norgasis23 (Bay of Biscay); 11: Line3 (Labrador margin); 12: Platta nappe (fossil analogue, Alps); 13: Lanzo Massif (fossil analogue, Alps); 14: Chenaillet ophiolite (fossil analogue, Alps); 15: Axial valley of the Southwest Indian Ridge (present day analogue).

The results of our study provide a conceptual understanding of how serpentinization and magmatism may control strain distribution during mantle exhumation at distal margins and enable us to discuss the processes controlling the polyphase evolution of these domains. Unravelling the nature and significance of these intra-basement reflectors and their potential role as decoupling interfaces provides new insights into the processes controlling the transition from exhumation of subcontinental mantle to oceanic spreading.

2. Seismic observations: intra-basement reflections

In this section, we identify and characterize potential decoupling interfaces at Ocean Continent Transitions of magma-poor rifted margins. The studied areas are thus located between the edge of unambiguous continental and first oceanic crusts (Fig. 2). In this study we do neither investigate continental nor oceanic Mohos, nor the S-type reflections (localized landward of the continental crust termination) (Fig. 2). Except for the Iberia-Newfoundland rifted margins and the Tyrrhenian Sea where serpentinized peridotites have been drilled (Boillot et al., 1988; Bonatti et al., 1990; Sawyer et al., 1994; Whitmarsh et al., 1998; Tucholke et al., 2004), interpretation of basement nature in distal domains relies on reflection, refraction seismic data and/or potential field data, leading to a variety of propositions.

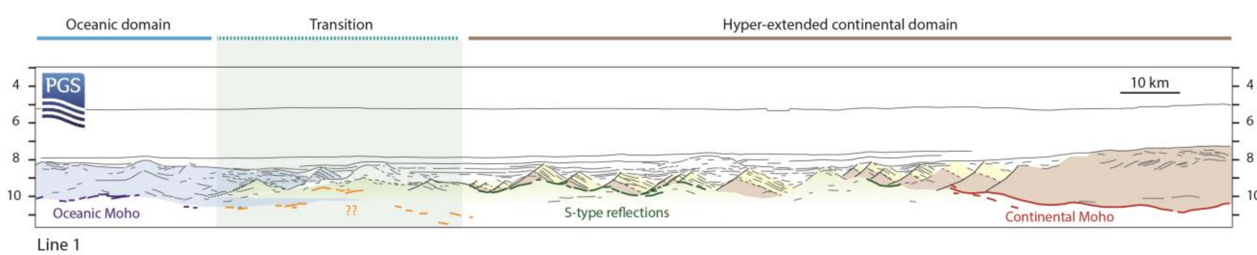

Figure 2: Seismic line drawing illustrating the main reflections that can be observed at magma-poor rifted margins and their locations. The area studied in this paper is highlighted in light green. Figure modified from Gillard et al. 2017. Seismic line located in the Gulf of Guinea.

On reflection seismic sections, the exhumed mantle domain is generally characterized by the absence of "pre-exhumation" (generally considered as "pre-rift") sediments (exceptions are extensional allochthons of continental origin) and the absence of clear and continuous Moho reflections (Minshull et al., 1998; Gillard et al., 2015). These criteria can help to differentiate this domain from the adjacent hyperextended continental and steady state oceanic crusts. Additional constraints may come from refraction seismic data. P-wave velocities can range between 4.5 and 7 km/s for the upper 2 to 4 km of basement, and an elevated velocity gradient of 1 s^{-1} is considered as characteristic for an exhumed mantle domain (Chian et al., 1999). Based on gravity inversion results that use a mean crustal density of 2850 $kg.m^{-3}$, a basement composed of exhumed serpentinized mantle would appear as an approximately 3 km thick crust (Cowie et al., 2015). This value contrasts with the thickness of standard magmatic oceanic crust (e.g. Penrose crust) (~7 km; White et al., 1992; Bown and White, 1994) and the oceanward decreasing thickness of hyperextended continental crust resulting in a wedge-shaped geometry (0 to 10 km, e.g. Aslanian et al., 2009; Nirrengarten et al., 2016). While the transition from hyperextended continental crust to exhumed mantle can be quite confidently distinguished, the transition to first steady state oceanic crust is more controversial (Peron-Pinvidic et al., 2016; Peron-Pinvidic and Osmundsen, 2016). This zone of uncertainty is currently referred to as “proto-oceanic domain” or “outer domain” (Gillard et al., 2015; Peron-Pinvidic and Osmundsen, 2016; Sauter et al., 2018; Gillard et al., 2017; Tugend et al., 2018).

2.1. Iberia-Newfoundland rifted margins

The Iberia-Newfoundland conjugate rifted margins resulted from Late Jurassic-Early Cretaceous rifting and opening of the southern North Atlantic (Tucholke et al. 2007; Nirrengarten et al., 2018). The Iberia-Newfoundland conjugate margins are considered as the type example of a magma-poor rift system because of the high density and diversity of the data sets acquired on these margins. In particular, the distal domains are well described and the presence of a zone of exhumed continental mantle is attested by several dredges (Boillot et al., 1980), ODP drill holes (Boillot et al., 1988; Sawyer et al., 1994; Whitmarsh et al., 1998; Tucholke et al., 2004) reflection seismic surveys (Pickup et al., 1996) and refraction seismic data (Dean et al., 2000; Funck et al., 2003; Whitmarsh et al., 1996).

Intra-basement reflections have been reported from the Screech 1 (Newfoundland margin) (Fig.3a) and IAM9 (Iberian margin) (Fig.3b) reflection seismic lines (Hopper et al., 2004, 2006; Pickup et al., 1996; Reston and McDermott, 2011) and occur in a domain where mantle is exhumed. On the Newfoundland margin, a strong reflection is visible (“Z reflection”; Hopper et al., 2004, 2006) at approximately 1 sec TWTT below top basement (Fig. 3c). To stay coherent with all the observations and to avoid confusion on the nature of the reflectors, we will refer to the Z reflector as “UR” (Upper Reflector). The basement above this reflector correlates with low P-wave velocities (4.3-4.5 km/s) (Funck et al., 2003). Note that the resolution in that area is really low, meaning that these velocities are badly constrained and that there is no mention about the velocity gradient in this layer. Immediately below the reflector, the underlying level shows P-wave velocities of 7.6 km/s gradually increasing with depth to 8.0 km/s (Funck et al., 2003). At the conjugate Iberia margin, a transparent upper basement layer is observed in the exhumed mantle domain (Pickup et al., 1996) (Fig. 3d). The thickness of this layer varies between 0.5 and 1 sec TWTT. It displays intermediate velocities (5.8-6.8 km/s) (Sibuet and Tucholke, 2012) and its base is marked by strong reflectivity. Based on seismic refraction analysis, Minshull et al. (2014) showed that the first 3 km of exhumed basement at the Iberia margin has a steeper velocity gradient (from 4.3 to 7.3 km/s) compared to the deeper 3 to 6 km of basement (7.3 to 7.9 km/s).

A key observation is that normal faults can generally be interpreted as rooting into the UR (e.g. Screech 1 line; Fig.3c). However, it can also be observed that the UR is sometimes back-tilted to the point that it reaches the top basement. That suggests that the UR can also be affected by new exhumation faults and potentially exhumed (Fig.3c).

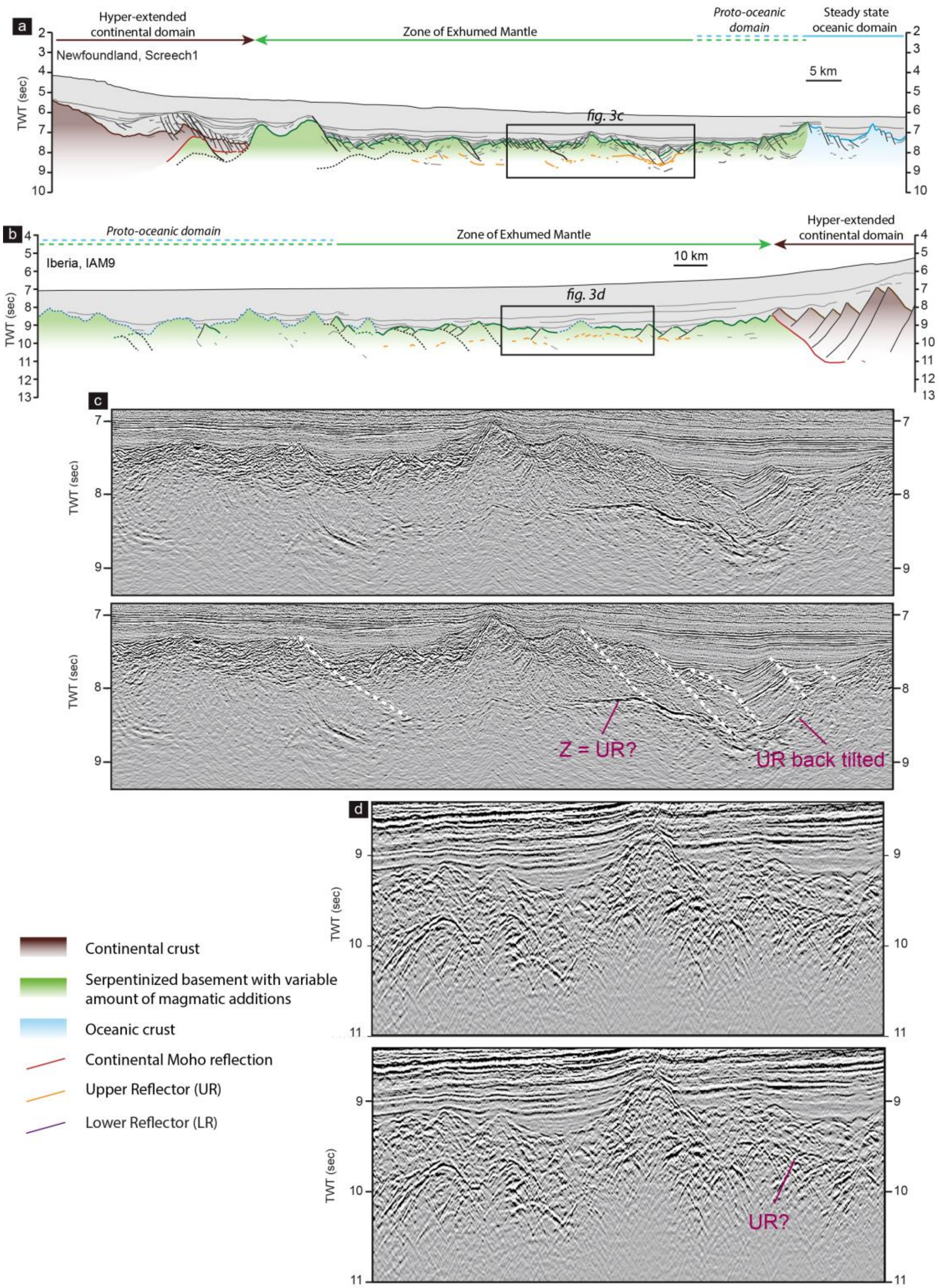

Figure 3: Conjugate examples of non interpreted and interpreted seismic sections at (a) the Newfoundland distal margin (Screech 1 line, interpretation from Gillard et al. 2016a) and (b) Iberian distal margin (IAM9 line). (c) and (d) Zooms of the

basement architecture in the zone of exhumed mantle at both margins, showing the presence of strong reflections (UR) at a depth between 0.5 and 1 sec TWT below top-basement. The IAM9 seismic section is from Pickup et al. 1996.

2.2.East Antarctica rifted margin off Wilkes Land

Rifting between Australia and Antarctica is postulated to have started during Callovian time (around 164 Ma; Totterdell et al., 2000) and rifting is recognized as polyphase (Ball et al., 2013; Gillard et al., 2015). However, the age of final breakup and first oceanic crust is currently debated (Williams et al., 2019). The presence of high-quality seismic reflection data enabled the architecture of the ultra-distal domains to be interpreted as formed by a wide zone of exhumed mantle (Sayers et al., 2001; Direen et al., 2011; Ball et al., 2013; Gillard et al., 2015). This interpretation is supported, at the western termination, by dredges of serpentinized mantle rocks in the Diamantina Zone (Beslier et al., 2004).

Similar to the UR observed at the Iberia-Newfoundland margins, the Antarctic seismic sections from AGSO survey GA228 (Stagg and Schiwy, 2002) show strong reflections localized at 1 sec TWTT below top-basement (Fig. 4a, b). These reflections are often sub-horizontal (Fig. 4c, d). They are more or less continuous throughout the exhumed mantle domain. In the Zone of Exhumed Mantle, the interpreted normal faults generally root into the UR. However, in the most distal part (i.e., proto-oceanic domain of Gillard et al., 2015) we observe a change in the morphology of this reflector. Indeed, UR is deformed, with a similar morphology to top basement, which is marked by fault bounded, highly rotated blocks (Fig. 4e). Further oceanward, an increase in extrusive magmatic additions is interpreted to seal normal faults that formerly affected the exhumed basement (Gillard et al., 2016a) (Fig. 5a, c). In this domain, some normal faults offset the UR and penetrate deeper into the basement (Fig. 5c, 6b).

In addition to the UR, a second set of reflections is observed at this margin. These reflections, hereafter referred to as the “LR” (Lower Reflectors), are generally observed between 1.5 and 2 sec TWTT below the top basement (Fig. 5c, d, 6c). These deeper reflections are more subdued and sparsely visible only in the interpreted proto-oceanic domain, close to the transition with the first steady state oceanic crust. In contrast to the UR whose occurrence is always correlated with the presence of normal faults, only few major faults also root on the LR (Fig.5c, 6c). Where it is the case, the UR is offset (Fig. 6e). It finally appears that at some locations in the proto-oceanic domain, the UR and the LR can be observed together (Fig. 5a, b; 6b).

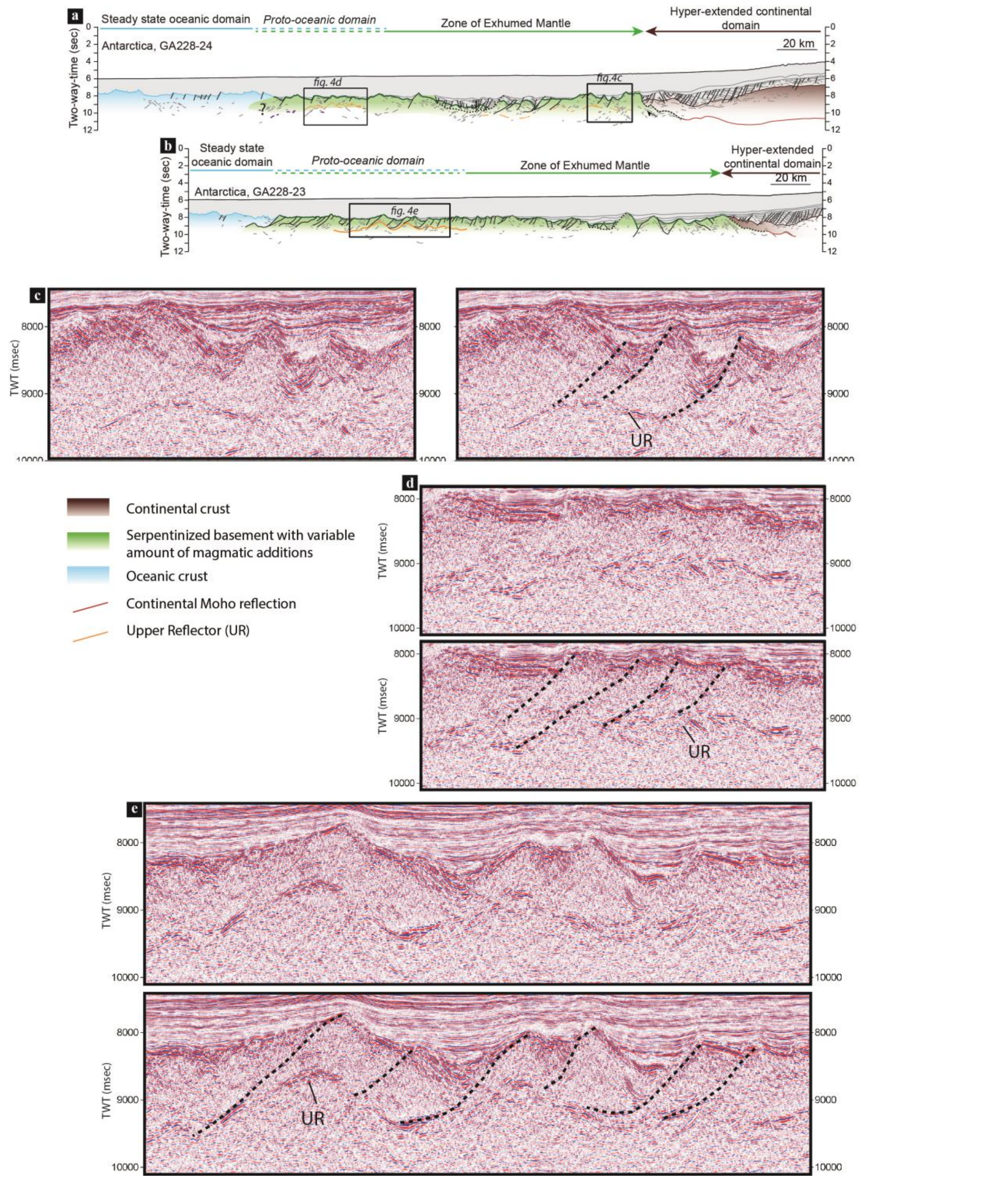

Figure 4: Examples of non interpreted and interpreted seismic sections at the East Antarctica distal margin (interpretation from Gillard 2014). (a) Line GA228-24, (b) Line GA228-23. (c), (d), (e) show zooms displaying the architecture of the basement in the Zone of Exhumed mantle (c) and in the proto-oceanic domain (d) and (e) with the presence of UR. ***Copyright Commonwealth of Australia (Geoscience Australia)***

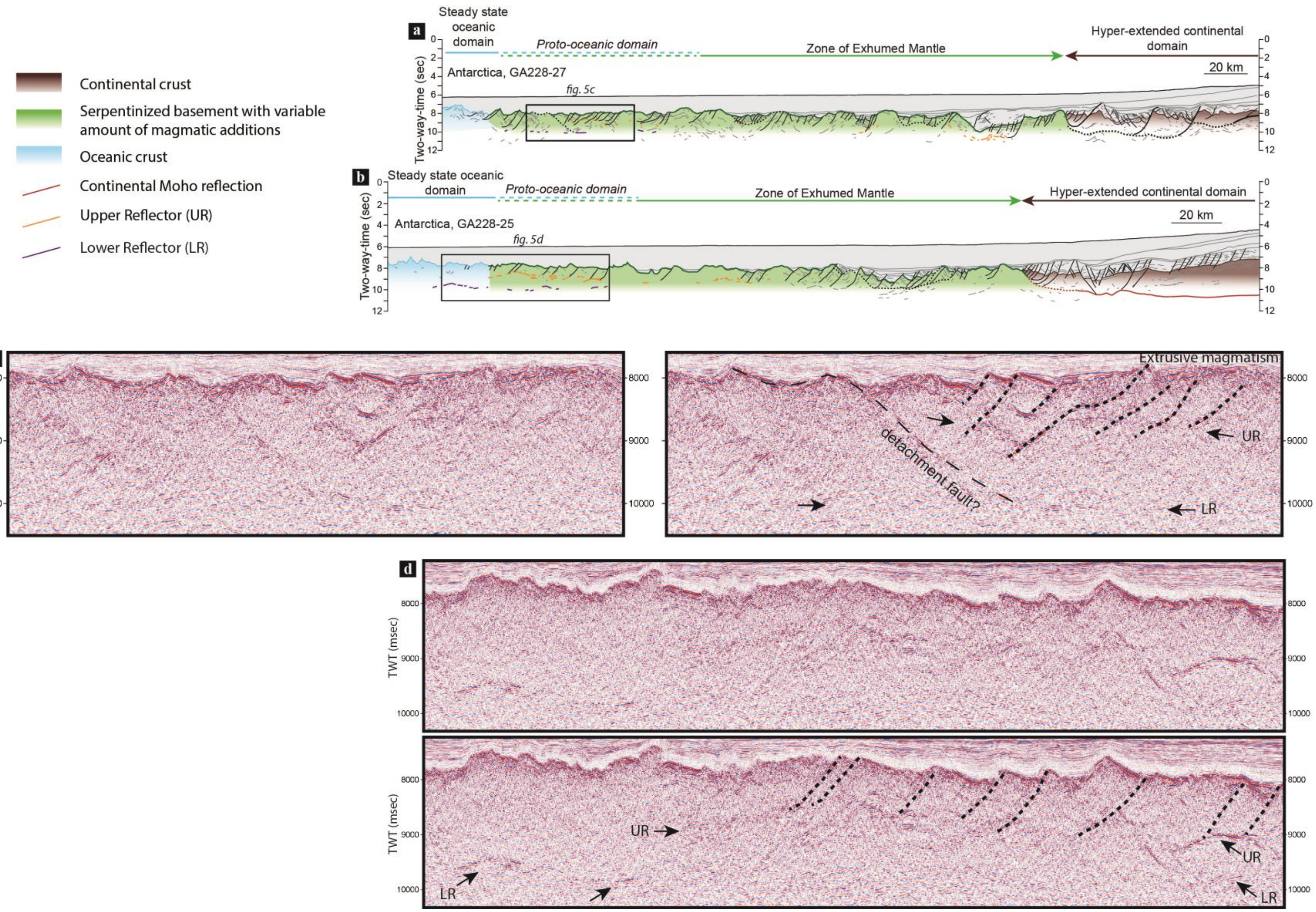

Continental crust
Serpentinized basement with variable amount of magmatic additions
Oceanic crust
Continental Moho reflection
Upper Reflector (UR)
Lower Reflector (LR)
a
Steady state oceanic domain
Proto-oceanic domain
Zone of Exhumed Mantle
Hyper-extended continental domain
Antarctica, GA228-27
fig. 5c
20 km
Two-way-time (sec)
b
Antarctica, GA228-25
fig. 5d
c
TWT (msec)
Extrusive magmatism
detachment fault?
UR
LR
d

Figure 5: Examples of non interpreted and interpreted seismic sections at the East Antarctica distal margin (interpretation from Gillard 2014). (a) Line GA228-27, (b) Line GA228-25. (c) and (d) show zooms of the basement architecture in the proto-oceanic domain with the presence of UR and LR. *Copyright Commonwealth of Australia (Geoscience Australia).*

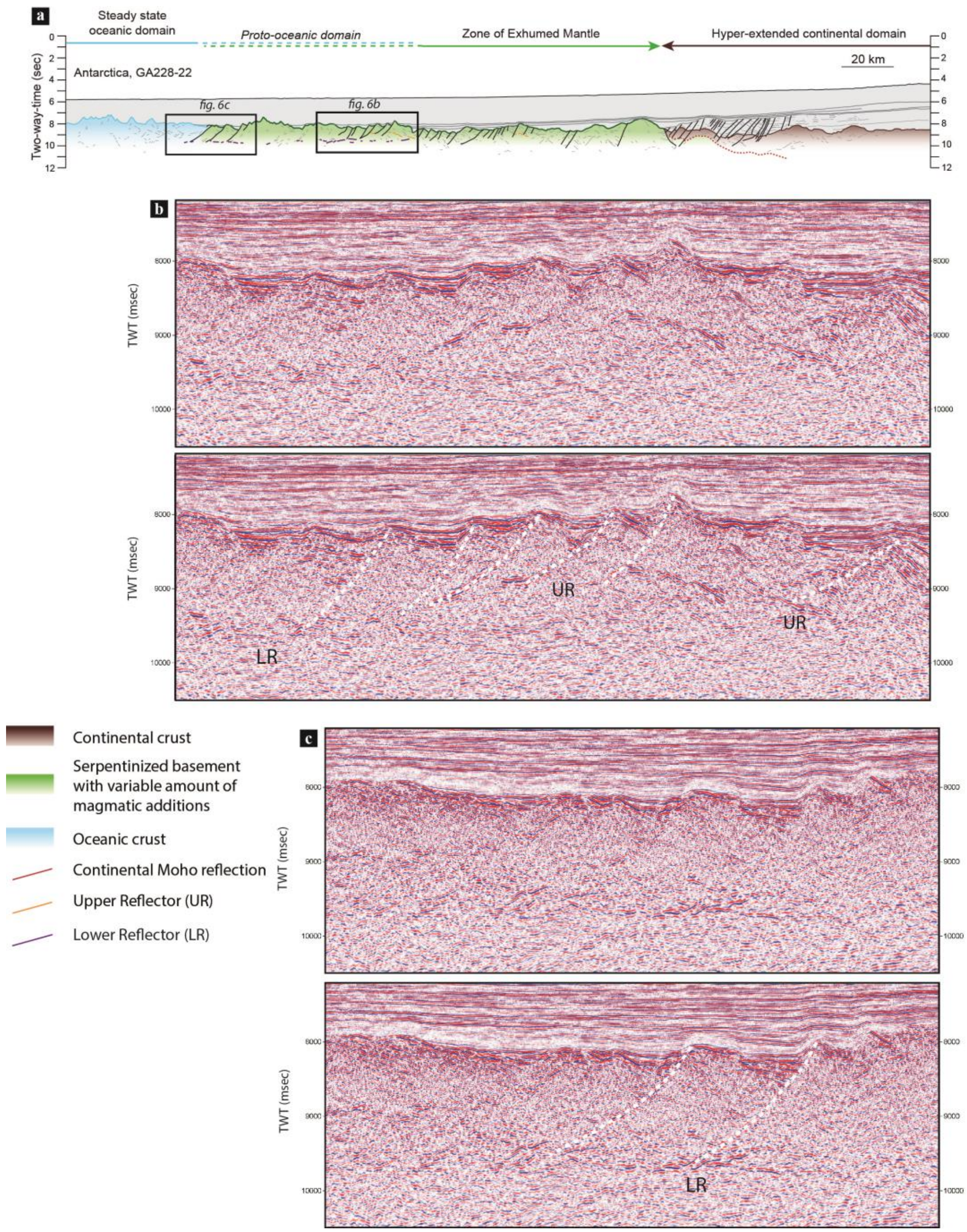

a
Steady state oceanic domain
Proto-oceanic domain
Zone of Exhumed Mantle
Hyper-extended continental domain
Two-way-time (sec)
Antarctica, GA228-22
20 km
fig. 6c
fig. 6b
b
TWT (msec)
UR
UR
LR
c
LR
Continental crust
Serpentinized basement with variable amount of magmatic additions
Oceanic crust
Continental Moho reflection
Upper Reflector (UR)
Lower Reflector (LR)

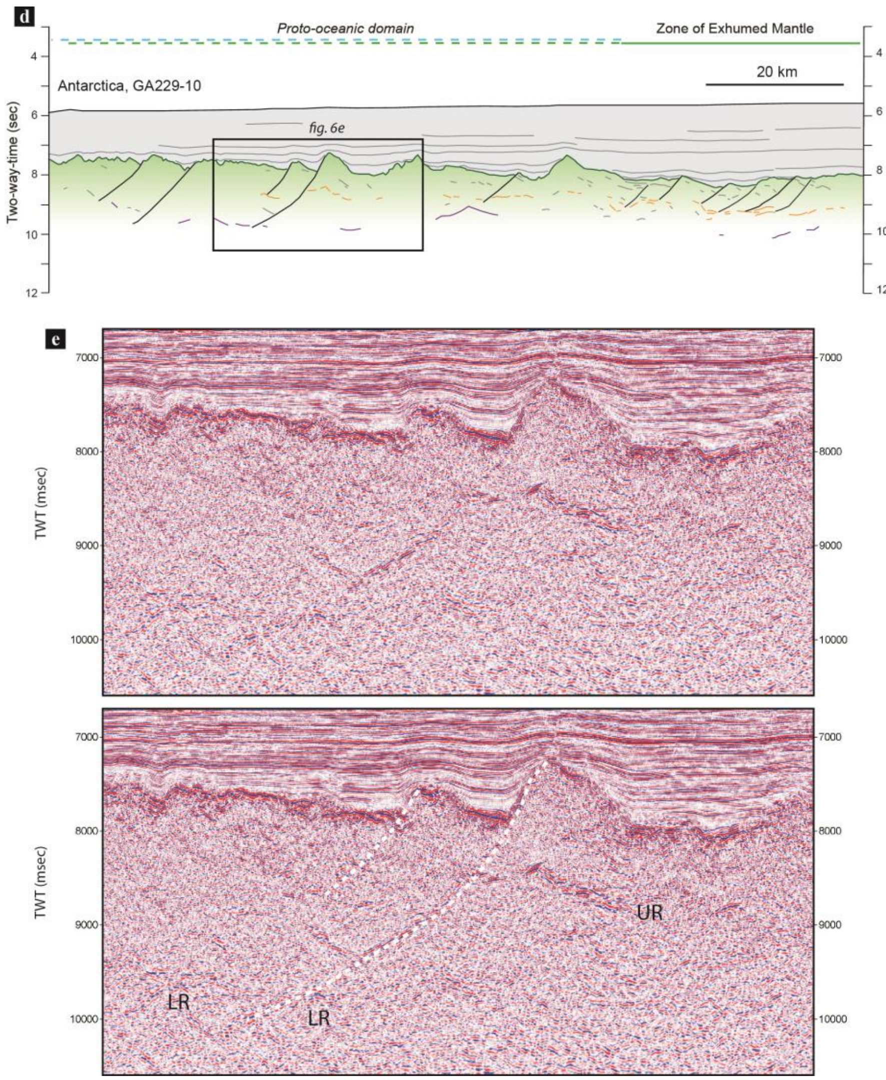

Figure 6 : Examples of non interpreted and interpreted seismic sections at the East Antarctica distal margin (interpretation from Gillard 2014). (a) Line GA228-22, (b) and (c) show zooms of the basement architecture in the proto-oceanic domain with the presence of UR and LR. (d) Line GA229-10, (e) zoom of the basement architecture in the proto-oceanic domain with the presence of normal faults rooting onto a deep reflector (LR?), UR appears back tilted by the fault. *Copyright Commonwealth of Australia (Geoscience Australia).*

2.3. East Antarctica rifted margin off Enderby Land

The margin off Enderby Land formed during the opening between East India and East Antarctica. Seafloor spreading in this area is thought to start in early Cretaceous (Gaina et al. 2007; Gibbons et al.

2013). Along this margin, the transition to steady state oceanic crust is clear and marked by a reflector interpreted as the oceanic Moho (Fig. 7). This transition is also characterized by a step up of the top basement and by a major change in the basement seismic character. The basement located south of this transition is intensely faulted, with irregular intra-basement reflections and no visible seismic reflection Moho. This basement has been referred to as a “transitional crust” (Stagg et al., 2004) and its nature has not been determined. It is supposedly continental in origin (Stagg et al., 2004) and/or composed by exhumed mantle (Gaina et al., 2007). The basement architecture is similar to that observed in the zone of exhumed mantle in the previous examples (e.g. Fig. 6). It contrasts with the adjacent 2s TWTT thick oceanic crust marked by a flat top basement and internal structure typical of magmatic oceanic crust (two sub-horizontal layers: a transparent upper crust, and a highly reflective lower crust). We note an increase of the extrusive magmatic supply near the step up marking the onset of oceanic crust. In particular, the basement in the interpreted zone of exhumed mantle and proto-oceanic domain contains high amplitude, horizontal reflections at 1s TWTT below the top basement, very similar to the UR previously observed. Normal faults also root into that reflection (Fig. 7).

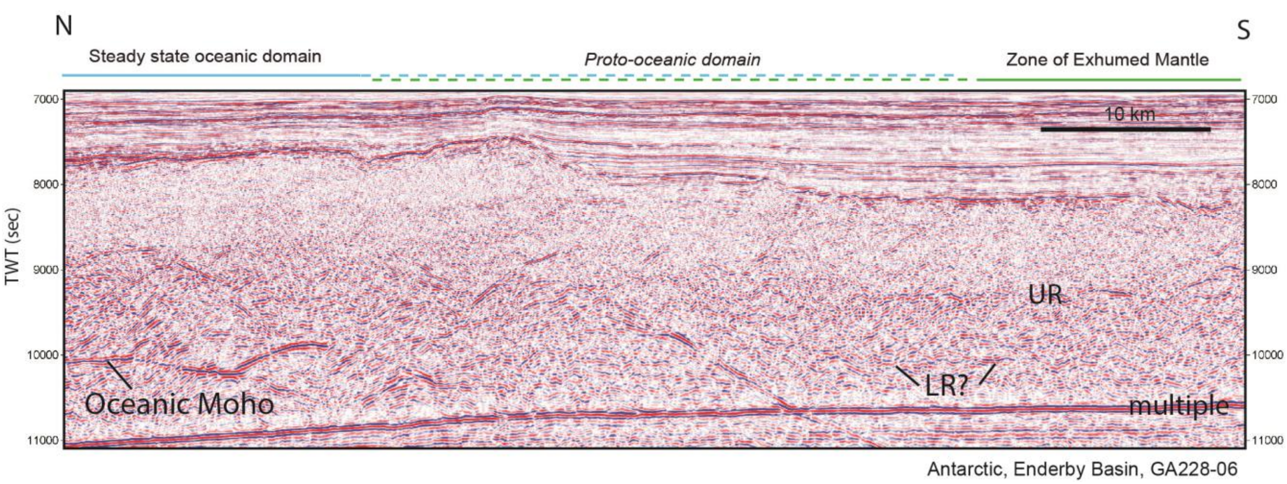

Figure 7: Seismic profile along the Antarctica margin, in the Enderby Basin, showing the transition between the proto-oceanic domain and the steady state oceanic domain. ***Copyright Commonwealth of Australia (Geoscience Australia)*****.**

2.4. The Armorican rifted margin (northern Bay of Biscay)

The Bay of Biscay corresponds to a V-shape oceanic basin, bordered to the north by the Western Approaches and Armorican margins. Following latest Jurassic to Early Cretaceous rifting, spreading initiated in late Aptian to early Albian and stopped in the Campanian (e.g. Tugend et al., 2015; Montadert et al., 1979). The first-order structure of the distal Armorican margin is constrained from both seismic observations (Thinon et al., 2003) and gravity inversions (Tugend et al., 2014) indicating the potential occurrence of a zone of exhumed serpentinized mantle between hyperextended continental and oceanic crusts.

Detailed seismic observations from the distal Armorican margin show different types of intra-basement reflectors (Thinon et al., 2003). Here, we focus our observations along the exhumed mantle domain of the NE-SW oriented Norgasis 23 seismic profile (Avedik and Olivet, 1994; Thinon et al., 2003) (Fig. 8a and c). In this domain, the upper part of the basement is poorly reflective, being relatively transparent and delimited at its base by discontinuous strong reflectors, located about ~1 s below the interpreted top basement and roughly parallel to it (referred to “MS” in Thinon et al., 2003). The location of this reflector in the exhumed mantle domain as well as its depth below top basement (about 1s) is comparable to the UR described in the previous sections.

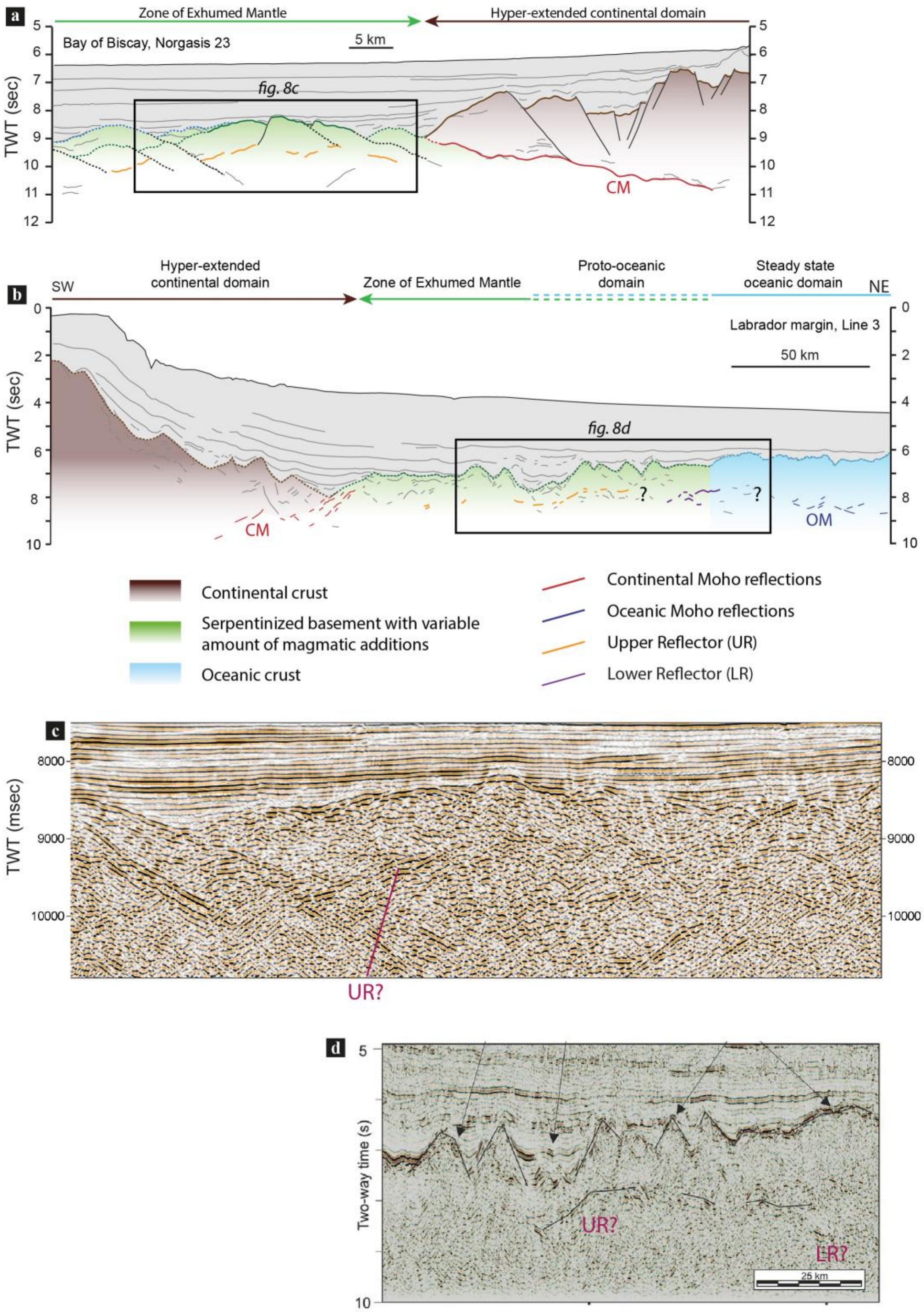

Figure 8: Interpreted seismic sections at (a) the Bay of Biscay (Norgasis 23 Line) and at (b) the Labrador margin (Line 3). CM: Continental Moho, OM: Oceanic Moho. The uninterpreted Norgasis 23 seismic section is available from Avedik and Olivet, 1994 and was previously published in Thinon et al. 2003 and Labrador line 3 seismic section is from Keen et al. 2017. (c) Zoom of the

basement architecture along the Norgasis 23 line showing the UR. (d) zoom modified from Keen et al. 2017 showing the basement architecture and the presence of shallow reflections (comparable to UR).

2.5. The Labrador rifted margin

Rifting along the central Labrador margin initiated during the Early Cretaceous and breakup occurred in Maastrichtian or Paleocene time (e.g., Oakey and Chalmers, 2012). Wide-angle reflection/refraction data suggest the presence of a domain of exhumed serpentinized mantle (Chian et al., 1995; Keen et al., 1994, 2017). Discontinuous reflectors are visible below the top basement in the domains interpreted by Keen et al. (2017) as the zone of exhumed mantle and the proto-oceanic domain (Fig. 8b). These reflectors have been previously described by Chian et al. (1995) and referred to as "D" reflections. Even if the reflectors are more discontinuous, it is here again possible to interpret two sets of reflections: UR and LR (Fig. 8d).

2.6. A present-day analogue: the axial valley of the Southwest Indian Ridge

The easternmost part of the Southwest Indian Ridge (SWIR) is known to exhibit a smooth seafloor that is almost entirely composed of seawater-altered mantle-derived rocks that were brought to the surface by exhumation faults on both sides of the ridge axis over the last 10 Ma (Sauter et al. 2013). Recent seismic acquisition in such an area of exhumed mantle shows the presence of several sets of intra-basement reflections within the axial valley of the SWIR at 64°36'E (Momoh et al. 2017) (Fig.9): south-dipping, north-dipping and sub-horizontal reflectors. The sub-horizontal reflectors occur just below the top basement (1 in Fig. 9), and between 1.5 sec TWTT (2 in Fig. 9) and 2 sec TWTT below top basement (3 in Fig. 9). While the south-dipping reflectors have been interpreted as the active axial exhumation fault, the nature of the other sets of reflectors is less constrained. Some of the north-dipping reflectors are not reaching top basement and seem to be sealed by the shallowest group of sub-horizontal reflectors, which are interpreted as magmatic sills (Momoh et al. 2017). These north-dipping reflectors also appear to root on the top of the deepest group of sub-horizontal reflectors. These observations can be explained, similarly to those reported from the Antarctica margin (see Fig. 5c), as normal faults affecting the oceanic exhumed basement and rooting onto a decoupling level. The base of the deepest group of sub-horizontal reflectors is located approximately at 2 sec TWTT below top basement and correlates with the 7.5 km/sec velocity contour, which marks the transition from serpentinized to fresh peridotites. The way these reflectors can be compared to the UR and LR will be discussed later.

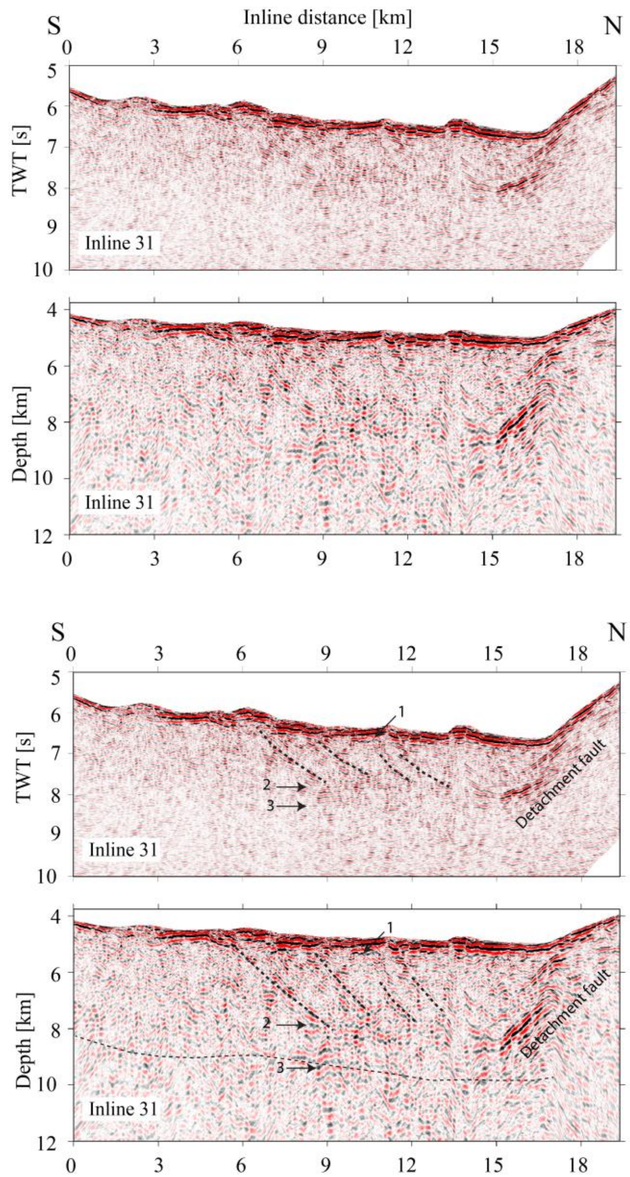

Figure 9: North-south time-migrated and depth-converted seismic sections imaging the axial valley of the Southwest Indian Ridge at 65°36’E (Momoh et al. 2017). In this area, dredge hauls that targeted the top basement recovered 97% serpentinized peridotites (Sauter et al. 2013). Small patches of lavas are erupted directly onto the detachment surface. Thin dashed black line represents the 7.5 km/s velocity contour (Momoh et al. 2017).

3. Nature and origin of intra-mantle basement interfaces: constraints from geological observations and quantitative analyses

Our observations suggest that the UR and LR can be interpreted as distinct rooting levels for normal faults, and thus correspond to different decoupling interfaces (décollement levels). However, their nature and origin remain unclear from seismic observations only. Several hypotheses are possible to explain these décollements, such as (1) detachment/exhumation fault planes, (2) shear zones, (3) brittle-ductile transitions, (4) serpentinization fronts, (5) top of intrusive magmatic bodies (e.g., relict magma chambers). All these décollement levels are potentially present in ultra-distal domains of magma-poor rifted margins. As the mantle is likely exhumed and serpentinized in our case studies, we investigate the evolution of the physical properties of serpentinized mantle rocks to interpret the potential nature of the UR and the LR. Additional evidence of physical properties comes from outcrops that we consider as field analogues for the LR.

3.1. Physical proprieties of serpentinized mantle rocks

The hydration of mantle peridotites by seawater penetration along fault planes corresponds to the serpentinization process, a reaction that occurs under a wide range of temperatures (from <100° up to 350°C) (Bonatti et al., 1984; Agrinier and Cannat, 1997; Mével, 2003; Decitre et al., 2002). During mantle exhumation along a detachment fault the serpentinization process initially starts along the fault zone at depths of 3 to 6km below top basement before propagating away from the fault plane, simultaneously with volumetric expansion related to progressive unloading during footwall unroofing and rotation (Andreani et al., 2007). When reaching the seafloor, mantle rocks are already strongly serpentinized. This process leads to the formation of a basement with crustal p-wave velocities ranging between 4.5 and <8 km/s depending on the degree of serpentinization (Fig. 10). Strongly serpentinized peridotites at the top basement progressively evolve into non-serpentinized peridotites at depth, as permeability reduces and temperature increases. From a petrological point of view, there is no sharp boundary between serpentinized and non-serpentinized mantle peridotites. In this sense, there is neither a Moho nor a crust-mantle boundary in domains of exhumed mantle (Minshull et al., 1998). Serpentinization also reduces the density compared to unaltered peridotite (from 3.3 to 2.5 g/cm^3) (O'Hanley, 1996). It coincides with a decrease of seismic velocities, from 8 to 7.5 km/s between 6 and 3 km below the top basement, and from 7.5 to 5 km/s from 3 km below top basement to the top basement (Miller and Christensen, 1997) (Fig.10). These velocity ranges are comparable to what can be observed from refraction seismic studies for the upper and lower basement layers at the Iberia-Newfoundland margins for example (Chian et al., 1999; Dean et al., 2000).

However, despite the absence of a clear Moho discontinuity, intra-basement reflectors can still be observed in the exhumed mantle and the outer/proto-oceanic domains of magma-poor rifted margins on time migrated seismic sections, as shown previously (Fig. 3 to 8). Based on the refraction data of Minshull et al. (2014) for the Iberia exhumed mantle domain, we can consider a velocity range of 4.3-7.3 km/s for basement above UR (located at 1 sec TWT below top basement) and a velocity range of 7.3-7.9 km/s for basement between UR and LR (located at 2 sec TWT below top basement). These velocities allow us to calculate depth ranges for UR and LR: UR can be inferred to occur at 2.15 to 3.65 km below top basement and LR at 5.8 to 7.6 km below top basement. It is interesting to note that the depth range of UR coincides with abrupt changes in the mantle rock properties (Fig.10). Indeed, the evolution of the degree of serpentinization is not linear; serpentinization quickly decreases from the top basement (about 100%) to about 3 km depth, i.e. the depth-range of the UR, where it reaches ~15%. Below, it evolves more gently before reaching the maximum depth of serpentinization (that is ~0%) at ~6.5 km, corresponding to the depth-range of the LR (Fig.10). This maximum depth of serpentinization in exhumed mantle domains is based on velocity measurements (e.g. Cole et al., 2002) and may coincide with the 450-500°C isotherm, which represents the serpentine-olivine equilibrium temperature at ~0.2 GPa (Ulmer and Trommsdorff, 1999). Moreover, 15% serpentinization at a depth of approximately 3 km corresponds to a major change in the mechanical behavior of hydrated peridotite (Fig.10). Indeed, the mechanical strength is very low between complete and 15% serpentinization and rises abruptly for degrees < 15% approaching the strength of unaltered dunite (Escartín et al., 2001). This abrupt change is related to the fact that serpentine is mechanically much weaker than olivine and pyroxene, and has very low coefficients of friction (0.3 compared to 0.85 for unaltered peridotite) (Escartín et al., 2001). Brittle deformation in hydrated peridotite is thus efficiently accommodated by shear cracks in the serpentinite (Escartín et al., 1997), even for low degrees of serpentinization (Escartín et al., 2001). These results show that a major rheological interface is expected to occur at a depth of approximately 3 km below top basement in exhumed mantle domains.

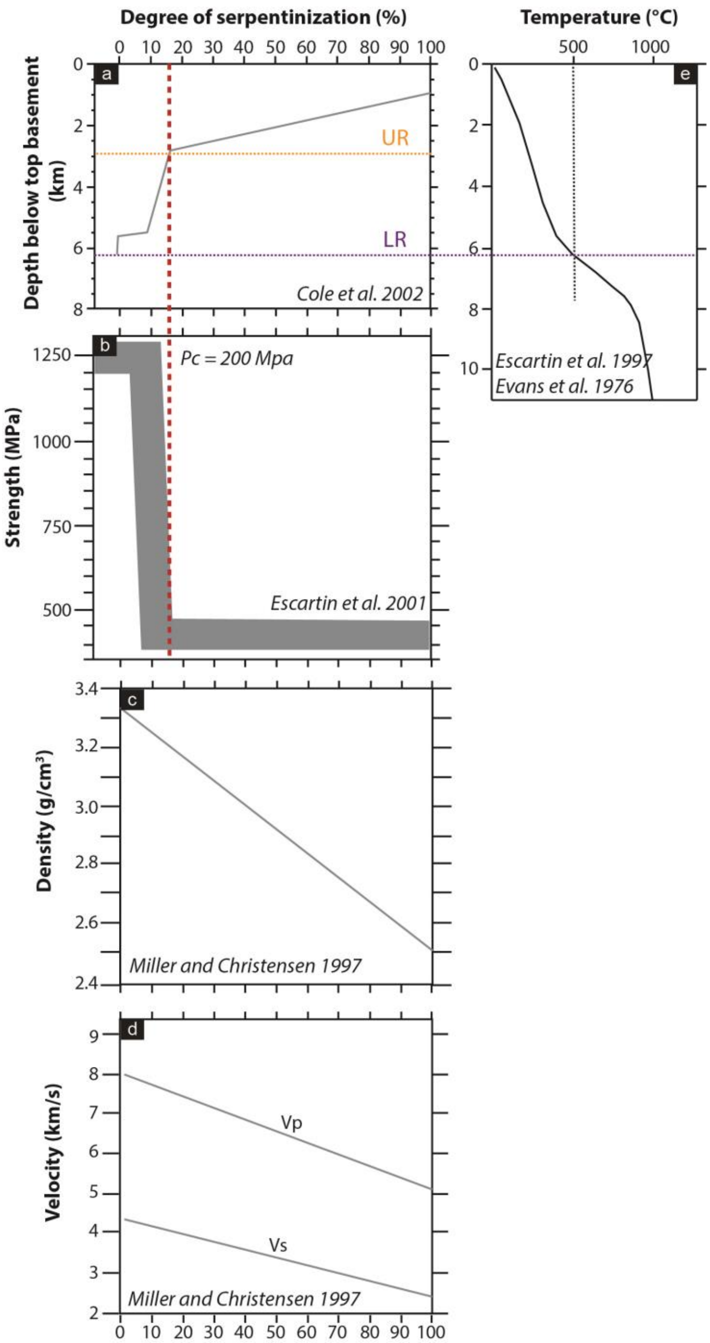

Figure 10: Physical properties of serpentinized mantle rocks: (a) evolution of the degree of serpentinization with depth (from Cole et al. 2002), predicted from the velocity model of Dean et al. (2000) and following the relationship between velocity and serpentinization found by Miller and Christensen (1997) ; (b) evolution of the strength in function of the degree of serpentinization (from Escartin et al. 2001); (c) evolution of the density; and (d) velocity in function of the degree of serpentinization (from Miller and Christensen 1997); (e) evolution of the temperature with depth (from Escartin et al. 1997).

The abrupt change in the strength is highlighted in red and correlates with the depth of UR. The maximum depth of serpentinization is highlighted in violet and correlates with the depth of the LR.

3.2. Upper Reflector (UR): a major rheological interface

The non-linear evolution of the degree of serpentinization with depth resulting in an abrupt change in the mechanical behavior of hydrated peridotite at about 15% can explain the occurrence of a décollement level at the depth where UR is observed (1 sec TWTT, Fig. 5). This décollement may represent a major rheological interface created by the modification of the strain accommodation in the serpentinized peridotite for serpentinization degree reaching approximately 15%. A seismic reflector (UR) at the depth of this interface is likely the result of the combined effects of serpentinization and deformation. Normal faults root into the previously created rheological interface and connect networks of serpentinized mantle. This process enhances the formation of fault rocks (gouges) at the intersection between normal faults and the rheological interface, in a similar way than proposed by Schuba et al. (2018) for the S-reflector at the Galicia margin. Schuba et al. (2018) show that the reflection along the S-interface has been created by a fault zone of 60 to 230m thick. In their attempt to model the seismic reflectivity along the Tasna detachment fault, Hölker et al (2002) suppose a similar average thickness of 70m for the fault zone at the top of the serpentinized peridotite and show that the seismic reflection can be caused by the slow-to-fast velocity transition at the base of the damaged zone. That means that the reflectivity could not have been created by the velocity contrast marking the transition between the continental crust and the serpentinized peridotite damaged zone, but by intra-serpentinized peridotite velocity transition thanks to the presence of the damage zone, which is more comparable to our case study. In our study, similar thicknesses of the fault zone along the rheological interface could thus result in the observed seismic reflections (UR). Moreover, the faults in the hanging wall will allow the water to easily penetrate at this level, leading to hydration of the interface and resulting in additional serpentinization and strain weakening. A similar process has been described by Bayrakci et al. (2016) along the hyper-extended continental crust at the Galicia margin. It is likely that the presence of this hydrated interface controls the deformation within the exhumed mantle. An alternative hypothesis is that the UR represents the detachment fault plane buried under rider blocks (or extensional allochthons) in the rolling hinge model (e.g. Buck 1988; Reston et al. 2007; Ranero and Reston 2011). The rolling hinge model would imply that the UR is strictly of the same age than the normal faults rooting onto it. On the contrary, in the first hypothesis the decoupling interface is created by a previous phase of mantle exhumation and can be substantially older than the development of the normal faults. The observations that in the proto-oceanic domain the UR is affected and cross-cut by normal faults (Fig. 4e, 5c, 6e) is for us inconsistent with the rolling hinge model. Therefore, we favor the hypothesis that the UR is a rheological boundary related to serpentinization processes.

3.3. Lower Reflector (LR): a hydrothermal boundary or a major shear zone in the mantle? Constraints from the Lanzo peridotite (Western Alps/N-Italy)

The LR, located at 2 sec TWTT (between 5.8 and 7.6 km) below top basement, appears to coincide with the maximum depth of serpentinization, i.e. the “serpentinization front”. However, we do not expect to observe this hydrothermal boundary on seismic sections since it does not coincide with an abrupt change in the mineralogy of the mantle peridotite. Indeed, in contrast to the 15% interface, no clear rheological discontinuity is expected to occur at the serpentinization front (Fig.10). In addition, the depth of the serpentinization front is not necessarily stable (Cole et al., 2002), as it depends on a variety of parameters such as permeability, thermal gradient and access to water. For example, upper mantle peridotites at depth > 6 km below seafloor can be within the temperature range of serpentinization in the case of a significant cooling effect caused by water circulation into the fault zones (Maffione et al., 2014). However, on seismic sections, it can be observed that the rooting level of some faults corresponds with a reflector (LR, Fig. 5, 6), suggesting the presence of a decollement level at 2s TWTT. If the serpentinization process cannot account for this observation, other processes, such as magmatism and/or shear zones may explain the LR. This reflector is too deep to be directly drilled at present day rifted margins. The only way to investigate further the nature of the LR is to study fossil analogues.

Here we consider the Lanzo shear zone as a potential analogue of the LR observed on seismic sections from magma-poor rifted margins. The Lanzo shear zone is exposed in the Lanzo massif in northwestern Italy, north of Torino (Fig. 11a). The Lanzo massif is composed of weakly to fully serpentinized peridotites, exhumed during the opening of the Jurassic Alpine Tethys ocean (Müntener and Piccardo, 2003; Kaczmarek and Müntener, 2008; Nicolas et al., 1972; Kaczmarek and Müntener, 2010). The Lanzo shear zone corresponds to a kilometer-scale, mylonitic shear zone juxtaposing weakly serpentinized, melt impregnated plagioclase peridotites (Lanzo Central) (Kaczmarek and Müntener, 2008; Nicolas et al., 1972; Bodinier, 1988) against more serpentinized mantle rocks (Lanzo North) (Fig. 11b). Similar shear zones in mantle peridotites have also been observed in the Ligurian ophiolites (Northern Apennines, Italy; Tribuzio et al., 1995), in the Erro Tobbio peridotites (Hoogerduijn Strating et al. 1991) or in the Platta unit (Müntener et al. 2010). Microstructural evidence indicates that these shear zones were active at high temperature (700 to 900°C), with low or no involvement of seawater-derived fluids (Tribuzio et al., 1995; Sanfilippo and Tribuzio, 2011). The ductile deformation occurred therefore deeper in the mantle, below the serpentinization front, associated with mantle exhumation and/or magma-emplacement. Indeed, the formation and evolution of the Lanzo shear zone appears strongly related to melt-rock reactions coupled with active deformation (Müntener and Piccardo, 2003; Kaczmarek and Müntener, 2008, 2010; Higgie and Tommasi, 2014). Progressive deformation is witnessed by the development of textures evolving from porphyroclastic to fine-grained porphyroclastic, to proto-mylonitic, to ultramylonitic (Kaczmarek and Müntener, 2008; Kaczmarek and Tommasi, 2011). Mineral chemistry, microstructures and thermometry of the Lanzo shear zone suggest that strain localization began at temperature > 1000°C in the lithospheric mantle (Kaczmarek and Müntener, 2008), i.e. at depth of approximately 12-15 km (pressure of 4.4 kbar, Fumagalli et al., 2017) (Fig. 11c). In particular, it appears that melt rock reaction in the subcontinental mantle started before the onset of the high-temperature shearing, favoring localization of deformation (Holtzman et al., 2003; Kohlstedt and Holtzman, 2009; Holtzman and Kendall, 2010). The degree of deformation and strain localization along the Lanzo shear zone progressively increases together with the decrease of the pressure and temperature and with grain size reduction (Kaczmarek and Müntener, 2008; Fumagalli et al., 2017; Linckens et al., 2011) (Fig. 11c). This suggests a progressive uplift of the shear zone at shallower lithospheric levels. The actively deforming shear zone appears to focus migrating liquids and then to act as a permeability barrier due to grain size reduction. The plagioclase peridotite mylonites observed along the Lanzo shear zone formed at ~3 kbars, thus approximately at 9 km depth (Fumagalli et al., 2017) and below ~850°C (Kaczmarek and Müntener, 2008). It is interesting to note that the dynamically recrystallised ultra-mylonites locally contain retrograde Cl-rich hydrous minerals (amphibole and chlorite, Vieira Duarte, *personal communication*) that formed at temperatures higher than the serpentine stability (Kaczmarek and Müntener, 2008), suggesting that the shear zone finally reached the base of the hydrothermal front, i.e. about 6 to 7km as is the case for the LR. This suggests that during the latest stage of the margin evolution, the mylonitic shear zone can also coincide with the rooting level of late exhumation faults, which can locally penetrate and exhume the shear zone to the seafloor. An example of an exhumed mylonitic shear zone is observed at the Chenaillet Ophiolite (Manatschal et al., 2011), where Jurassic gabbros show a high temperature mylonitic shear zone truncated by low temperature, hydrated fault zones corresponding to extensional detachment faults. The mylonites and ultramylonites observed in the gabbros formed at temperatures between 700°C to 800°C (Mevel et al., 1978), i.e. at similar conditions like those observed along the Lanzo shear zone. Moreover, the Chenaillet mylonites show evidence for syn-tectonic magmatism that have been affected by fluids after exhumation of the rocks along the shear zone (Mevel et al., 1978; Manatschal et al., 2011). The scale of the Lanzo shear zone, which is about 1 km wide, makes this structure an interesting case for its interpretation as an analogue of the LR. The presence of a sub-horizontal mylonitic shear zone in the peridotite flooring the serpentinization front could indeed explain the origin of the LR in the proto-oceanic domain. Moreover, the melts percolating at the level of the shear zone will also likely create the impedance contrast necessary to obtain seismic reflections at this level. The Lanzo shear zone provides an explanation for large-scale decoupling horizons between the serpentinized and non-serpentinized, plagioclase-bearing mantle peridotites.

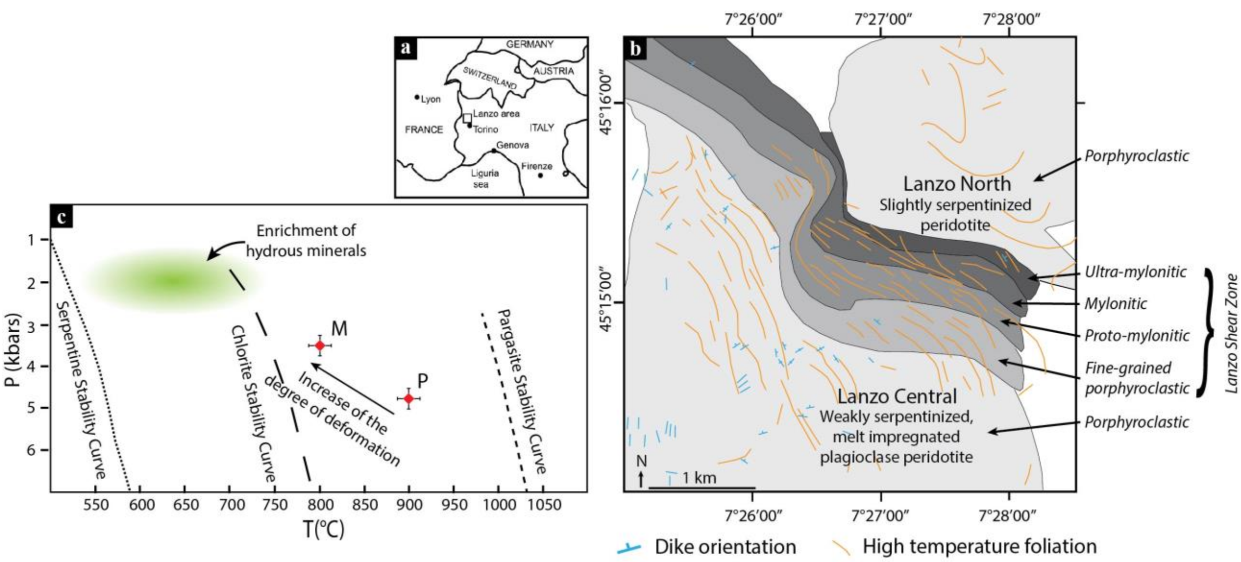

Figure 11: (a) Location of the Lanzo massif. (b) Map of the Lanzo Shear Zone modified from Kaczmarek and Müntener, 2008. (c) Simplified Pressure-Temperature diagram illustrating the evolution of the deformation for the Lanzo Shear Zone and the beginnings of hydration above serpentine stability (P: porphyroclastic textures; M: mylonitic textures; Pargasite stability after Niida and Green, 1999; Chlorite and serpentine stability after Ulmer and Trommsdorff, 1999). Pressure-temperature estimates and errors (± 0.5 kbars and ± 25°C) of the plagioclase peridotite are from the FACE barometer (Fumagalli et al., 2017).

4. Discussion

4.1. Serpentinization and accommodation of extensional deformation

Seismic and field studies show the presence of two major distinct decoupling levels in the basement of ultra-distal domains at magma-poor rifted margins. These decoupling levels are at different depths and appear to be associated with different processes. In the upper part of the lithosphere, extension is manifested by mantle exhumation along detachment faults. The serpentinization process occurring along these active exhumation faults leads to the formation of a major rheological interface at approximately 3 km below seafloor. This efficient decollement level is highlighted by the presence of numerous normal faults rooting into this interface (UR, Fig. 4). This rheological interface thus appears to be a key factor for the organization of the deformation during the mantle exhumation stage. Indeed, it allows mechanical decoupling between the shallowest, brittle/frictional part of the lithosphere, and deeper levels that accommodate the deformation along mylonitic shear zones.

In our hypothesis the decoupling surface at 3 km below seafloor will allow for a constant re-organization of the deformation due to exhumation and serpentinization in the upper part of the continental lithosphere (Gillard et al., 2015, 2016b, 2016a). This is associated with magma emplacement and thermal perturbations in the lower part of the continental lithosphere (Fig. 12). The complex interaction between the upper and lower parts of the continental lithosphere, and the successive rising of the asthenosphere may explain the transition from asymmetric structures during early exhumation to finally symmetric structures during lithospheric breakup (Gillard et al., 2016b).

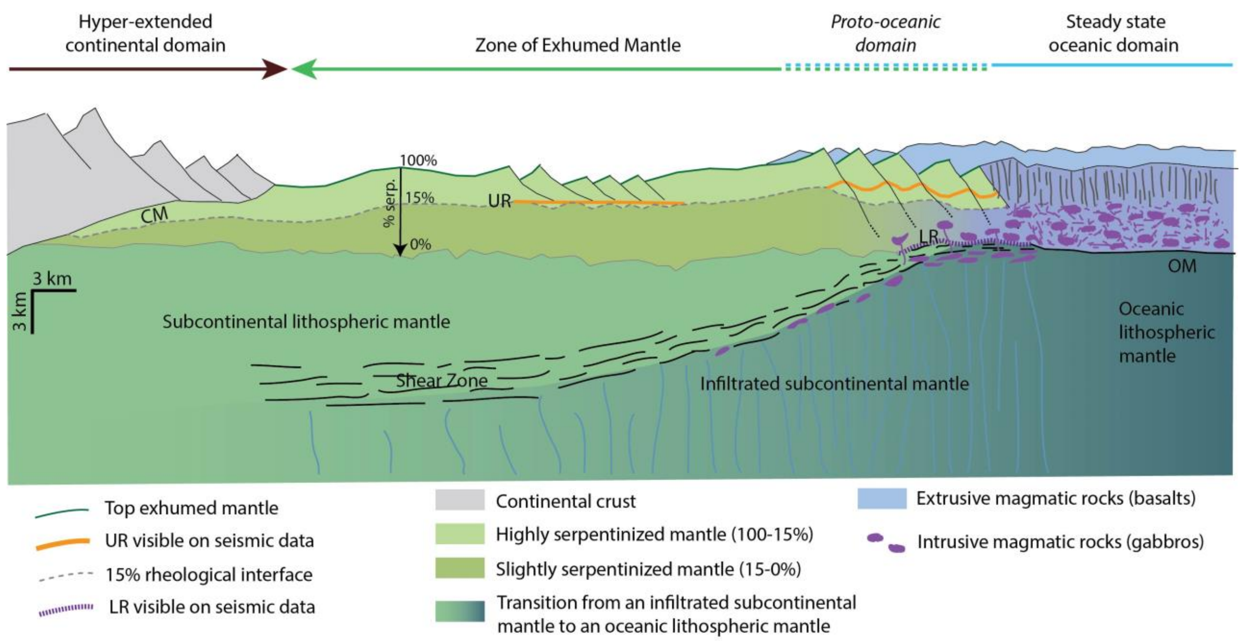

Figure 12: Snapshot summarizing at a final stage the main observations and the processes leading to the formation of the interfaces UR and LR. CM: Continental Moho; OM: Oceanic Moho.

The thinning of the continental lithosphere, associated with mantle exhumation, will passively uplift the deep shear zone, from depth of 12-15 km to the base of the hydrothermal front (6-10 km) (Kaczmarek and Müntener, 2008) (Fig.12). Indeed, contrary to previous studies proposing that exhumation faults were lithospheric-scale structures rooting at the lithosphere-asthenosphere boundary (Lemoine et al., 1987; Boillot and Froitzheim, 2001; Wernicke, 1981), several observations from oceanic core complexes and fossil rifted margins argue for a shallower rooting depth (6-10 km), at or just below the hydrothermal front (deMartin et al., 2007; Manatschal et al., 2011).

Our observations from seismic reflection and field studies suggest that during the first stage of mantle exhumation, faults are rooting on decoupling levels controlled by the degree of serpentinization. The accommodation is thus mainly tectonic and controlled by hydration reactions (Fig. 12, 13). However, during the development of the proto-oceanic domain, the UR is deformed by faults that seem to root at deeper levels (Fig. 6, 12). This evolution is associated with an increase of the magmatism extruded on top of the basement (Fig. 5a, c) and with the progressive appearance of the LR. These observations suggest that magmatism could play a key role in developing the new interface controlling the rheology of extending mantle during the formation of the proto-oceanic domain and final breakup.

4.2. Distribution of magmatic rocks and influence on the structural evolution

The proto-oceanic domain show increasing evidence for of magmatic rocks at the top basement and is marked by the appearance of a deep reflector (LR) on seismic sections (Fig. 6). However, the presence of magmatic material at the top basement also suggests that part of magmatic material must also be stored at depth. Indeed, the emplacement level of magmatic rocks is partly controlled by buoyancy forces; magma might stagnate at levels of neutral buoyancy until they have fractionated and reacted to the point where magma density is less than that of the surrounding host rock (Ryan, 1993). Another possibility is that magma migration terminates when reaching an actively deforming "freezing horizon" (Morgan and Chen, 1993; Kohlstedt and Holtzman, 2009; Sparks and Parmentier, 1994). In this case, there could be a link between magma emplacement and strain localization. This last interpretation would be coherent with the observations made at the Lanzo Shear Zone (Kaczmarek and Müntener, 2008). Indeed, Kaczmarek and Müntener (2008) and Higgie and Tommasi (2014) showed that small gabbro dikes and sills are mainly distributed below, and sometimes parallel to the mylonitic shear zone in the Lanzo peridotite (Fig. 11). The reduction of permeability associated with the formation of the mylonite, perhaps coupled to the cooling effects of the hydrothermal front, could form a thermal boundary controlling the upward migration and crystallization of mafic melts in the proto-oceanic domain. The net result is the emplacement of gabbro sills during shearing (Kaczmarek and Müntener, 2008) at or just below the hydrothermal front, i.e. close to the depth of the LR. In addition to the fact that the LR could represent a shear zone, the presence of intrusive magmatic material along this horizon could also explain its reflectivity. The sub-horizontal reflectors observed between 1 and 2 sec TWTT below top basement in the axial valley of the SWIR (Fig. 9) have been interpreted as magmatic intrusions above the transition from fresh to serpentinized peridotites (Momoh et al. 2017). However, the observation that normal faults are rooting onto these reflectors (Fig. 9) indicates some analogy with the UR reflections observed at the different studied magma-poor rifted margins. Indeed, the thermal, magmatic and hydration conditions occurring at the SWIR are comparable to the ones that occurred during the evolution of the exhumed mantle domain at magma-poor rifted margins, leading to the development of similar serpentine-related structures such as the UR. In contrast, it is not clear if the deepest reflectors in the oceanic basement at the SWIR can be compared to the LR observed at magma-poor rifted margins. Indeed, the very low magmatic budget recognized at the SWIR (Sauter et al. 2013) is likely different to the one involved during the development of the proto-oceanic domain, where the LR occurred. This latest domain should rather be compared with Oceanic Core Complexes, which are recognized as more magmatic systems than the exhumed mantle domains of the SWIR (Tucholke et al. 2008). In addition, strong subhorizontal reflectors have been observed in reflection images at the Rainbow Core Complex (Mid-Atlantic Ridge), at approximately 6 km below top basement, where mantle derived rocks have been dredged (Dunn et al. 2017; Canales et al. 2017). These reflectors have been interpreted as cooling melt bodies intruded into the massif, their heat driving the fluid circulation (Dunn et al., 2017). It would be interesting to deeply investigate the comparison between the LR and intrusive magmatic bodies at Oceanic Core Complexes. However, it is possible that the LR is a structure specific to magma-poor rifted margins, as we propose that it is linked both to the increasing magmatic budget and to a shear zone associated to the processes of continental lithospheric extension.

Similar to what has been proposed for the Rainbow Core Complex (Dunn et al. 2017), we propose that the presence of partially molten intrusions close to the hydrothermal front will change the thermal and hydration conditions in the proto-oceanic domain of the studied magma-poor margins. As a consequence, the rheological structure of the basement is transient, and normal faults are able to penetrate deeper than the UR and possibly connect to the LR (Fig. 6, 12). Moreover, it has been observed on seismic sections that extrusive magmatism in the proto-oceanic domain is often present at the breakaway of these normal faults (Fig. 6). This is similar to what has been mapped in field analogues (Chenaillet Ophiolite), where it has been suggested that normal faults act as feeder systems for extrusive magmatism (Manatschal et al., 2011). We propose that in this domain, normal faults are able to penetrate sufficiently deep to extract melt stored along the LR interface.

4.3. Synthesis of the structural and magmatic evolution

We summarize here the key steps in the structural and magmatic evolution of the distal domain at magma-poor rifted margins in the conceptual model shown in Fig. 13.

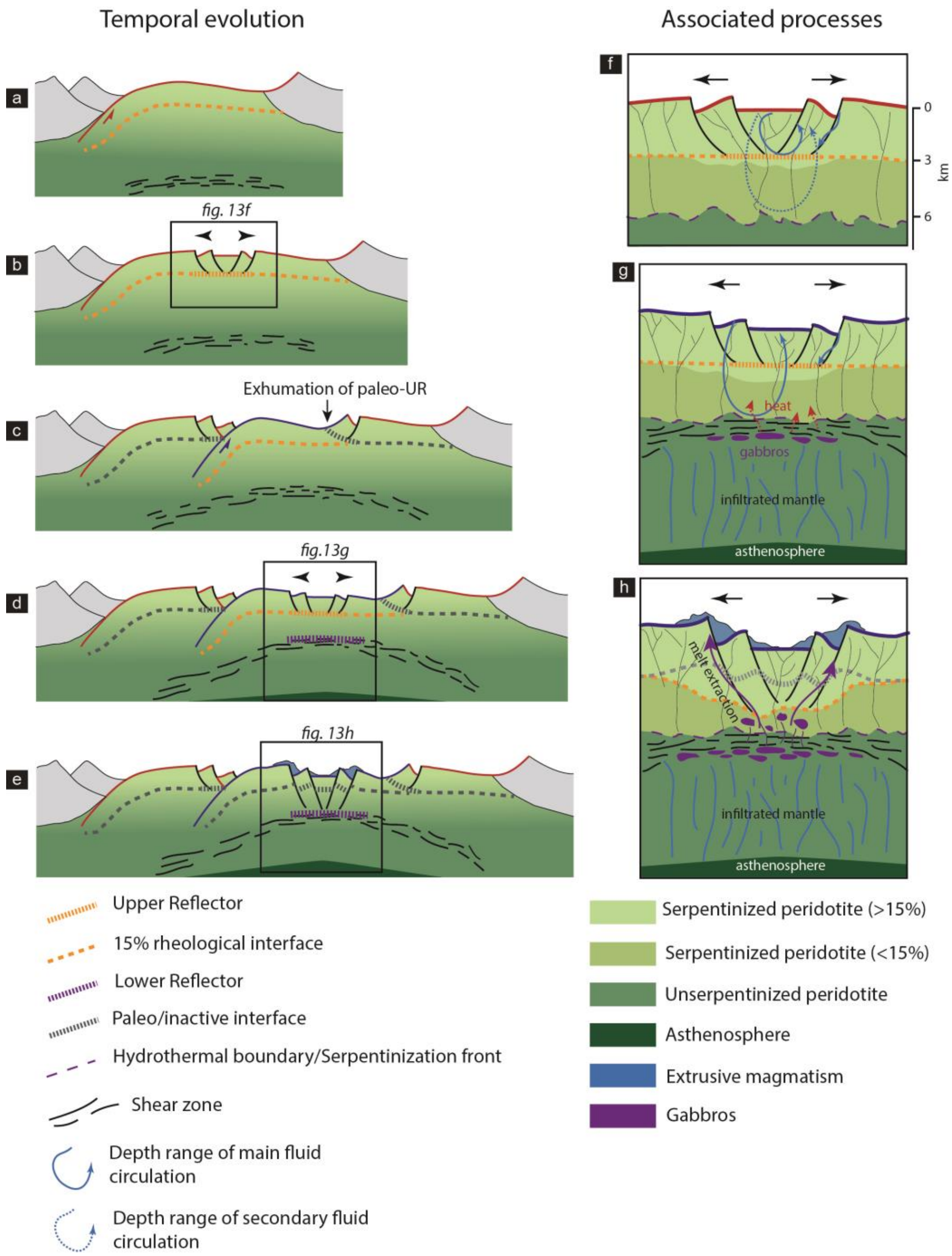

Figure 13: Geologic model showing the temporal evolution of the distal margin with specific focus on the formation and evolution of the different decoupling interfaces in distal domains of magma-poor rifted margins. Zooms highlighting the processes (hydration, shearing, magmatism) and their interactions associated to the formation/evolution of the decoupling interfaces.

Following the hyperextension stage, the separation of the continental crust occurs in a magma-poor context, leading to an accommodation of the extension by mantle exhumation along detachment faults (Fig. 13a). At depth, the thinning of the lithosphere is accommodated by the formation of a wide shear zone. The strain localization at depth is favored by melt-rock reactions. The hydration process associated with detachment faulting leads to the formation of a strong rheological interface at the level of 15% of serpentinite, which is approximately located at a depth of 3 km below seafloor (Fig. 13a). The exhumation fault becomes progressively inactive and extensional deformation tends to migrate in the area where the asthenosphere is rising (Fig. 13b). This re-organization of the deformation is controlled by the activation of the rheological interface that is used as a decoupling level for normal faults (visible as UR on seismic sections) (Fig. 13f). The fluid circulation along active normal faults can lead to a new generation of serpentinization just below the pre-existing UR interface, probably preconditioning the initiation of a new exhumation fault (Fig. 13c). At this stage, the UR can be exhumed at the top-basement as a paleo-decoupling interface (Fig.3; 13c). As extension and mantle exhumation continues, extensional deformation along the deep shear zone will localize and evolve towards the formation of peridotite mylonites as the shear zone is progressively exhumed at shallower depths and lower temperatures. As the subcontinental lithosphere thins, melt infiltration in the mantle below the shear zone will increase (Picazo et al., 2016), but the reduction of the permeability in the shear zone will act as a barrier for the upward melt migration. The shear zone will finally reach the base of the hydrothermal front, which can be approximately at 6-7 km (Fig.13d). At this stage, the presence of plagioclase peridotite and/or partially crystallized gabbroic bodies just below the hydrothermal front will impact the rheology of the upper serpentinized layer (Fig. 13g). Normal faults are thus able to penetrate deeper and to extract some of the melt, which was stored at depth (Fig. 13e, h). In reaching the hydrothermal front, the shear zone also reaches the depth where it can be sampled by potential new exhumation faults. It is thus possible to exhume infiltrated mantle at the seafloor, represented by plagioclase peridotite, re-fertilized by melt percolation, as observed for example in the Platta nappe or Chenaillet Ophiolites (Muntener et al., 2004; Picazo et al., 2016; Muntener et al., 2010). This final stage could thus be referred to as the lithospheric breakup (Tugend et al., 2018; Peron-Pinvidic and Osmundsen, 2016), marking the end of rifting and recording the onset of seafloor spreading.

5. Conclusions

Based on seismic observations, we highlighted the presence of two main intra-basement decoupling interfaces in the exhumed mantle domain at magma-poor rifted margins. Integrating physical properties of serpentinized rocks and constraints from Alpine field analogues allowed us to interpret and discuss the nature and origin of these interfaces. In particular, our results show the presence of a strong rheological interface at about 3 km below top basement. We suggest that this interface played a major role in the organization of the deformation during the evolution of the exhumed mantle domain. The presence of a second, deeper interface occurring in the proto-oceanic domain seems to be the result of interactions between tectonic, hydrothermal and magmatic processes, which will modify the rheology of the serpentinized basement in this domain. It is interesting to note that during the formation of the proto-oceanic stage, the deformation of the upper and lower layers is progressively coupling, contrary to previous stages where the upper deformation was not directly linked to the deformation at depth. This change could be a signature of the proto-oceanic domain, together with the increase of magma emplacement at the seafloor. Indeed, this final coupling of the deformation, associated with the breakup of the continental lithosphere, marks the localization of the deformation and the initiation of a stable spreading center.

Acknowledgement

Seismic lines of the Antarctic surveys GA228 and GA229 were provided by Geoscience Australia after personal request and are published with the permission of Geoscience Australia. We also would like to thank I. Thinon and Ifremer for providing us the Norgasis 23 reflection seismic profile presented in this work. We kindly acknowledge Ekeabino Momoh for discussion and for the seismic image of the SWIR. This research was supported by Exxon Mobil as part of the CEIBA II project. We greatly thank Christopher A. Johnson and Anne-Marie Karpoff for useful and often in-depth discussions, as well as constructive comments by Tim Minshull and anonymous reviewers.

Bibliography

Agrinier, P., and Cannat, M., 1997, Oxygen-isotope constraints on serpentinization processes in ultramafic rocks from the Mid-Atlantic Ridge (23°N), *in* Karson, J.A., Cannat, M., Miller, D.J., and Elthon, D. eds., Proceedings of the Ocean Drilling Program, 153 Scientific Results, Ocean Drilling Program, Proceedings of the Ocean Drilling Program, v. 153, doi:10.2973/odp.proc.sr.153.1997.

Andreani, M., Mével, C., Boullier, A.-M., and Escartín, J., 2007, Dynamic control on serpentine crystallization in veins: Constraints on hydration processes in oceanic peridotites: Geochemistry, Geophysics, Geosystems, v. 8, p. Q02012, doi:10.1029/2006GC001373.

Aslanian, D. et al., 2009, Brazilian and African passive margins of the Central Segment of the South Atlantic Ocean: Kinematic constraints: Tectonophysics, v. 468, p. 98–112, doi:10.1016/j.tecto.2008.12.016.

Avedik, F., and Olivet, J.-L., 1994, Norgasis cruise, RV Le Nadir:, https://doi.org/10.17600/94000050.

Ball, P., Eagles, G., Ebinger, C., McClay, K., and Totterdell, J., 2013, The spatial and temporal evolution of strain during the separation of Australia and Antarctica: Geochemistry, Geophysics, Geosystems, v. 14, p. 2771–2799, doi:10.1002/ggge.20160.

Bayrakci, G. et al., 2016, Fault-controlled hydration of the upper mantle during continental rifting: Nature Geoscience, doi:10.1038/ngeo2671.

Beslier, M.O. et al., 2004, Une large transition continent-océan en pied de marge sud-ouest australienne: premiers résultats de la campagne MARGAU/MD110: Bulletin de la société Géologique de France, v. 175, p. 629–641.

Bodinier, J.L., 1988, Geochemistry and petrogenesis of the Lanzo peridotite body, western Alps: Tectonophysics, v. 149, p. 67–88, doi:10.1016/0040-1951(88)90119-9.

Boillot, G., and Froitzheim, N., 2001, Non-volcanic rifted margins, continental break-up and the onset of sea-floor spreading: some outstanding questions: Geological Society, London, Special Publications, v. 187, p. 9–30, doi:10.1144/GSL.SP.2001.187.01.02.

Boillot, G., Girardeau, J., and Kornprobst, J., 1988, Rifting of the Galicia margin: crustal thinning and emplacement of mantle rocks on the seefloor: Proceedings of the Ocean Drilling Program, Scientific Results, v. 103, p. 741–756.

Boillot, G., Grimaud, S., Mauffret, A., Mougenot, D., Kornprobst, J., Mergoil-Daniel, J., and Torrent, G., 1980, Ocean-continent boundary off the Iberian margin: A serpentinite diapir west of the Galicia Bank: Earth and Planetary Science Letters, v. 48, p. 23–34, doi:10.1016/0012-821X(80)90166-1.

Bonatti, E., Lawrence, J.R., and Morandi, N., 1984, Serpentinization of oceanic peridotites: temperature dependence of mineralogy and boron content: Earth and Planetary Science Letters, v. 70, p. 88–94, doi:10.1016/0012-821X(84)90211-5.

Bonatti, E., Seyler, M., Channell, J., Giraudeau, J., and Mascle, G., 1990, Peridotites drilled from the Tyrrhenian sea, ODP Leg 107, *in* Kastens, K.A., Mascle, J., and et al. eds., Proceedings of the Ocean Drilling Program, 107 Scientific Results, Ocean Drilling Program, Proceedings of the Ocean Drilling Program, v. 107, doi:10.2973/odp.proc.sr.107.1990.

Bown, J.W., and White, R.S., 1994, Variation with spreading rate of oceanic crustal thickness and geochemistry: Earth and Planetary Science Letters, v. 121, p. 435–449.

Buck, W.R., 1988, flexural rotation of normal faults: Tectonics, v. 7, p. 959–973, doi:10.1029/TC007i005p00959.

Canales, J.P., Dunn, R.A., Arai, R., and Sohn, R.A., 2017, Seismic imaging of magma sills beneath an ultramafic-hosted hydrothermal system: Geology, p. G38795.1, doi:10.1130/G38795.1.

Chian, D., Louden, K.E., Minshull, T.A., and Whitmarsh, R.B., 1999, Deep structure of the ocean-continent transition in the southern Iberia Abyssal Plain from seismic refraction profiles: Ocean Drilling Program (Legs 149 and 173) transect: Journal of Geophysical Research: Solid Earth, v. 104, p. 7443–7462, doi:10.1029/1999JB900004.

Chian, D., Louden, K.E., and Reid, I., 1995, Crustal structure of the Labrador Sea conjugate margin and implications for the formation of nonvolcanic continental margins: Journal of Geophysical Research: Solid Earth, v. 100, p. 24239–24253, doi:10.1029/95JB02162.

Cole, P.B., Minshull, T.A., and Whitmarsh, R.B., 2002, Azimuthal seismic anisotropy in a zone of exhumed continental mantle, West Iberia margin: Geophysical Journal International, v. 151, p. 517–533, doi:10.1046/j.1365-246X.2002.01781.x.

Cowie, L., Angelo, R.M., Kusznir, N.J., Manatschal, G., and Horn, B., 2015, The palaeo-bathymetry of base Aptian salt deposition on the northern Angolan rifted margin: constraints from flexural back-stripping and reverse post-break-up thermal subsidence modelling: Petroleum Geoscience, p. 2014– 087, doi:10.1144/petgeo2014-087.

Dean, S.M., Minshull, T.A., Whitmarsh, R.B., and Louden, K.E., 2000, Deep structure of the ocean-continent transition in the southern Iberia Abyssal Plain from seismic refraction profiles: The IAM-9 transect at 40°20′N: Journal of Geophysical Research: Solid Earth, v. 105, p. 5859–5885, doi:10.1029/1999JB900301.

Decitre, S., Deloule, E., Reisberg, L., James, R., Agrinier, P., and Mével, C., 2002, Behavior of Li and its isotopes during serpentinization of oceanic peridotites: Geochemistry, Geophysics, Geosystems, v. 3, p. 1–20, doi:10.1029/2001GC000178.

deMartin, B.J., Sohn, R.A., Canales, J.P., and Humphris, S.E., 2007, Kinematics and geometry of active detachment faulting beneath the Trans-Atlantic Geotraverse (TAG) hydrothermal field on the Mid-Atlantic Ridge: Geology, v. 35, p. 711–714, doi:10.1130/G23718A.1.

Desmurs, L., Manatschal, G., and Bernoulli, D., 2001, The Steinmann Trinity revisited: mantle exhumation and magmatism along an ocean-continent transition: the Platta nappe, eastern Switzerland: Geological Society, London, Special Publications, v. 187, p. 235–266, doi:10.1144/GSL.SP.2001.187.01.12.

Desmurs, L., Müntener, O., and Manatschal, G., 2002, Onset of magmatic accretion within a magma-poor rifted margin: a case study from the Platta ocean-continent transition, eastern Switzerland: Contributions to Mineralogy and Petrology, v. 144, p. 365–382, doi:10.1007/s00410-002-0403-4.

Direen, N.G., Stagg, H.M.J., Symonds, P.A., and Colwell, J.B., 2011, Dominant symmetry of a conjugate southern Australian and East Antarctic magma-poor rifted margin segment: Geochemistry Geophysics Geosystems, v. 12, p. 29 PP., doi:201110.1029/2010GC003306.

Dunn, R.A., Arai, R., Eason, D.E., Canales, J.P., and Sohn, R.A., 2017, Three-Dimensional Seismic Structure of the Mid-Atlantic Ridge: An Investigation of Tectonic, Magmatic, and Hydrothermal Processes in the Rainbow Area: Mid-Atlantic Ridge Seismic Structure: Journal of Geophysical Research: Solid Earth, v. 122, p. 9580–9602, doi:10.1002/2017JB015051.

Escartín, J., Hirth, G., and Evans, B., 1997, Nondilatant brittle deformation of serpentinites: Implications for Mohr-Coulomb theory and the strength of faults: Journal of Geophysical Research: Solid Earth, v. 102, p. 2897–2913, doi:10.1029/96JB02792.

Escartín, J., Hirth, G., and Evans, B., 2001, Strength of slightly serpentinized peridotites: Implications for the tectonics of oceanic lithosphere: Geology, v. 29, p. 1023–1026, doi:10.1130/0091-7613(2001)029<1023:SOSSPI>2.0.CO;2.

Fumagalli, P., Borghini, G., Rampone, E., and Poli, S., 2017, Experimental calibration of Forsterite–Anorthite–Ca-Tschermak–Enstatite (FACE) geobarometer for mantle peridotites: Contributions to Mineralogy and Petrology, v. 172, p. 38, doi:10.1007/s00410-017-1352-2.

Funck, T., Hopper, J.R., Larsen, H.C., Louden, K.E., Tucholke, B.E., and Holbrook, W.S., 2003, Crustal structure of the ocean-continent transition at Flemish Cap: Seismic refraction results: Journal of Geophysical Research, v. 108, p. 2531, doi:10.1029/2003JB002434.

Gaina, C., Müller, R.D., Brown, B., Ishihara, T., and Ivanov, S.V., 2007, Breakup and early seafloor spreading between India and Antarctica: Geophysical Journal International, v. 170, p. 151–169, doi:10.1111/j.1365-246X.2007.03450.x.

Gibbons, A.D., Whittaker, J.M., and Müller, R.D., 2013, The breakup of East Gondwana: Assimilating constraints from Cretaceous ocean basins around India into a best-fit tectonic model: Journal of Geophysical Research: Solid Earth, v. 118, p. 808–822, doi:10.1002/jgrb.50079.

Gillard, M., Autin, J., and Manatschal, G., 2016a, Fault systems at hyper-extended rifted margins and embryonic oceanic crust: Structural style, evolution and relation to magma: Marine and Petroleum Geology, v. 76, p. 51–67, doi:10.1016/j.marpetgeo.2016.05.013.

Gillard, M., Autin, J., Manatschal, G., Sauter, D., Munschy, M., and Schaming, M., 2015, Tectonomagmatic evolution of the final stages of rifting along the deep conjugate Australian-Antarctic magma-poor rifted margins: Constraints from seismic observations: Tectonics, v. 34, p. 2015TC003850, doi:10.1002/2015TC003850.

Gillard, M., Manatschal, G., and Autin, J., 2016b, How can asymmetric detachment faults generate symmetric Ocean Continent Transitions? Terra Nova, v. 28, p. 27–34, doi:10.1111/ter.12183.

Gillard, M., Sauter, D., Tugend, J., Tomasi, S., Epin, M.-E., and Manatschal, G., 2017, Birth of an oceanic spreading center at a magma-poor rift system: Scientific Reports, v. 7, p. 15072, doi:10.1038/s41598-017-15522-2.

Higgie, K., and Tommasi, A., 2014, Deformation in a partially molten mantle: Constraints from plagioclase lherzolites from Lanzo, western Alps: Tectonophysics, v. 615–616, p. 167–181, doi:10.1016/j.tecto.2014.01.007.

Hölker, A.B., Manatschal, G., Holliger, K., and Bernoulli, D., 2002, Seismic structure and response of ocean-continent transition zones: Marine Geophysical Researches, v. 23, p. 319–334.

Holtzman, B.K., and Kendall, J.-M., 2010, Organized melt, seismic anisotropy, and plate boundary lubrication: Geochemistry, Geophysics, Geosystems, v. 11, p. Q0AB06, doi:10.1029/2010GC003296.

Holtzman, B.K., Kohlstedt, D.L., Zimmerman, M.E., Heidelbach, F., Hiraga, T., and Hustoft, J., 2003, Melt Segregation and Strain Partitioning: Implications for Seismic Anisotropy and Mantle Flow: Science, v. 301, p. 1227–1230, doi:10.1126/science.1087132.

Hopper, J.R., Funck, T., Tucholke, B.E., Larsen, H.C., Holbrook, W.S., Louden, K.E., Shillington, D., and Lau, H., 2004, Continental breakup and the onset of ultraslow seafloor spreading off Flemish Cap on the Newfoundland rifted margin: Geology, v. 32, p. 93–96, doi:10.1130/G19694.1.

Hopper, J.R., Funck, T., Tucholke, B.E., Louden, K.E., Holbrook, W.S., and Christian Larsen, H., 2006, A deep seismic investigation of the Flemish Cap margin: implications for the origin of deep reflectivity and evidence for asymmetric break-up between Newfoundland and Iberia: Geophysical Journal International, v. 164, p. 501–515, doi:10.1111/j.1365-246X.2006.02800.x.

Kaczmarek, M.-A., and Müntener, O., 2008, Juxtaposition of Melt Impregnation and High-Temperature Shear Zones in the Upper Mantle; Field and Petrological Constraints from the Lanzo Peridotite (Northern Italy): Journal of Petrology, v. 49, p. 2187–2220, doi:10.1093/petrology/egn065.

Kaczmarek, M.-A., and Müntener, O., 2010, The variability of peridotite composition across a mantle shear zone (Lanzo massif, Italy): interplay of melt focusing and deformation: Contributions to Mineralogy and Petrology, v. 160, p. 663–679, doi:10.1007/s00410-010-0500-8.

Kaczmarek, M.-A., and Tommasi, A., 2011, Anatomy of an extensional shear zone in the mantle, Lanzo massif, Italy: Geochemistry, Geophysics, Geosystems, v. 12, doi:10.1029/2011GC003627.

Keen, C.E., Dickie, K., and Dafoe, L.T., 2017, Structural characteristics of the ocean-continent transition along the rifted continental margin, offshore central Labrador: Marine and Petroleum Geology, doi:10.1016/j.marpetgeo.2017.10.012.

Keen, C.E., Potter, P., and Srivastava, S.P., 1994, Deep seismic reflection data across the conjugate margins of the Labrador Sea: Canadian Journal of Earth Sciences, v. 31, p. 192–205, doi:10.1139/e94-016.

Kohlstedt, D.L., and Holtzman, B.K., 2009, Shearing Melt Out of the Earth: An Experimentalist's Perspective on the Influence of Deformation on Melt Extraction: Annual Review of Earth and Planetary Sciences, v. 37, p. 561–593, doi:10.1146/annurev.earth.031208.100104.

Lemoine, M., Tricart, P., and Boillot, G., 1987, Ultramafic and gabbroic ocean floor of the Ligurian Tethys (Alps, Corsica, Apennines): In search of a genetic imodel: Geology, v. 15, p. 622–625, doi:10.1130/0091-7613(1987)15<622:UAGOFO>2.0.CO;2.

Linckens, J., Herwegh, M., Müntener, O., and Mercolli, I., 2011, Evolution of a polymineralic mantle shear zone and the role of second phases in the localization of deformation: Journal of Geophysical Research, v. 116, doi:10.1029/2010JB008119.

Lymer, G., Cresswell, D.J.F., Reston, T.J., Bull, J.M., Sawyer, D.S., Morgan, J.K., Stevenson, C., Causer, A., Minshull, T.A., and Shillington, D.J., 2019, 3D development of detachment faulting during continental breakup: Earth and Planetary Science Letters, v. 515, p. 90–99, doi:10.1016/j.epsl.2019.03.018.

Maffione, M., Morris, A., Plümper, O., and van Hinsbergen, D.J.J., 2014, Magnetic properties of variably serpentinized peridotites and their implication for the evolution of oceanic core complexes: Geochemistry, Geophysics, Geosystems, v. 15, doi:10.1002/2013GC004993.

Manatschal, G., Sauter, D., Karpoff, A.M., Masini, E., Mohn, G., and Lagabrielle, Y., 2011, The Chenaillet Ophiolite in the French/Italian Alps: An ancient analogue for an Oceanic Core Complex? Lithos, v. 124, p. 169–184, doi:10.1016/j.lithos.2010.10.017.

Mével, C., 2003, Serpentinization of abyssal peridotites at mid-ocean ridges: Comptes Rendus Geoscience, v. 335, p. 825–852, doi:10.1016/j.crte.2003.08.006.

Mevel, C., Caby, R., and Kienast, J.-R., 1978, Amphibolite facies conditions in the oceanic crust: example of amphibolitized flaser-gabbro and amphibolites from the Chenaillet ophiolite massif (Hautes Alpes, France): Earth and Planetary Science Letters, v. 39, p. 98–108, doi:10.1016/0012-821X(78)90146-2.

Miller, D.J., and Christensen, N.I. 25. SEISMIC VELOCITIES OF LOWER CRUSTAL AND UPPER MANTLE ROCKS FROM THE SLOW-SPREADING MID-ATLANTIC RIDGE, SOUTH OF THE KANE TRANSFORM ZONE (MARK):, http://www-odp.tamu.edu/publications/153_SR/VOLUME/CHAPTERS/sr153_25.pdf (accessed June 2014).

Minshull, T.A., 2009, Geophysical characterisation of the ocean–continent transition at magma-poor rifted margins: Comptes Rendus Geoscience, v. 341, p. 382–393, doi:10.1016/j.crte.2008.09.003.

Minshull, T.A., Dean, S.M., and Whitmarsh, R.B., 2014, The peridotite ridge province in the southern Iberia Abyssal Plain: Seismic constraints revisited: Journal of Geophysical Research: Solid Earth, p. 2014JB011011, doi:10.1002/2014JB011011.

Minshull, T.A., Muller, M.R., Robinson, C.J., White, R.S., and Bickle, M.J., 1998, Is the oceanic Moho a serpentinization front? Geological Society, London, Special Publications, v. 148, p. 71–80, doi:10.1144/GSL.SP.1998.148.01.05.

Momoh, E., Cannat, M., Watremez, L., Leroy, S., and Singh, S.C., 2017, Quasi-3-D Seismic Reflection Imaging and Wide-Angle Velocity Structure of Nearly Amagmatic Oceanic Lithosphere at the Ultraslow-Spreading Southwest Indian Ridge: Journal of Geophysical Research: Solid Earth, v. 122, p. 2017JB014754, doi:10.1002/2017JB014754.

Montadert, L., Roberts, D.G., de Charpal, O., and Guennoc, P., 1979, Rifting and subsidence of the northern continental margin of the bay of biscay: Ocean Drilling Program : College Station, http://www.deepseadrilling.org/48/volume/dsdp48_54.pdf (accessed July 2014).

Morgan, J.P., and Chen, Y.J., 1993, The genesis of oceanic crust: Magma injection, hydrothermal circulation, and crustal flow: Journal of Geophysical Research: Solid Earth, v. 98, p. 6283–6297, doi:10.1029/92JB02650.

Muntener, O., Manatschal, G., Desmurs, L., and Pettke, T., 2010, Plagioclase Peridotites in Ocean-Continent Transitions: Refertilized Mantle Domains Generated by Melt Stagnation in the Shallow Mantle Lithosphere: Journal of Petrology, v. 51, p. 255–294, doi:10.1093/petrology/egp087.

Müntener, O., Pettke, T., Desmurs, L., Meier, M., and Schaltegger, U., 2004, Refertilization of mantle peridotite in embryonic ocean basins: trace element and Nd isotopic evidence and implications for crust–mantle relationships: Earth and Planetary Science Letters, v. 221, p. 293–308, doi:10.1016/S0012-821X(04)00073-1.

Müntener, O., and Piccardo, G.B., 2003, Melt migration in ophiolitic peridotites: the message from Alpine-Apennine peridotites and implications for embryonic ocean basins: Geological Society, London, Special Publications, v. 218, p. 69–89, doi:10.1144/GSL.SP.2003.218.01.05.

Nemcok, M., Sinha, S.T., Stuart, C.J., Welker, C., Choudhuri, M., Sharma, S.P., Misra, A.A., Sinha, N., and Venkatraman, S., 2013, East Indian margin evolution and crustal architecture: integration of deep reflection seismic interpretation and gravity modelling: Geological Society, London, Special Publications, v. 369, p. 477–496, doi:10.1144/SP369.6.

Nicolas, A., Bouchez, J.L., and Boudier, F., 1972, Interpretation cinematique des deformations plastiques dans le massif de Lherzolite de lanzo (Alpes piemontaises) — comparaison avec d'autres Massifs: Tectonophysics, v. 14, p. 143–171, doi:10.1016/0040-1951(72)90107-2.

Niida, K., and Green, D.H., 1999, Stability and chemical composition of pargasitic amphibole in MORB pyrolite under upper mantle conditions: Contributions to Mineralogy and Petrology, v. 135, p. 18–40, doi:10.1007/s004100050495.

Nirrengarten, M., Manatschal, G., Tugend, J., Kusznir, N., and Sauter, D., 2018, Kinematic Evolution of the Southern North Atlantic: Implications for the Formation of Hyperextended Rift Systems: Tectonics, p. 2017TC004495, doi:10.1002/2017TC004495.

Nirrengarten, M., Manatschal, G., Yuan, X.P., Kusznir, N.J., and Maillot, B., 2016, Application of the critical Coulomb wedge theory to hyper-extended, magma-poor rifted margins: Earth and Planetary Science Letters, v. 442, p. 121–132, doi:10.1016/j.epsl.2016.03.004.

Oakey, G.N., and Chalmers, J.A., 2012, A new model for the Paleogene motion of Greenland relative to North America: Plate reconstructions of the Davis Strait and Nares Strait regions between

Canada and Greenland: Journal of Geophysical Research: Solid Earth, v. 117, doi:10.1029/2011JB008942.

O'Hanley, D.S., 1996, Serpentinites: records of tectonic and petrological history: New York, Oxford University Press, Oxford monographs on geology and geophysics no. 34, 277 p.

Pérez-Gussinyé, M., and Reston, T.J., 2001, Rheological evolution during extension at nonvolcanic rifted margins: Onset of serpentinization and development of detachments leading to continental breakup: Journal of Geophysical Research: Solid Earth, v. 106, p. 3961–3975, doi:10.1029/2000JB900325.

Pérez-Gussinyé, M., Reston, T.J., and Morgan, J.P., 2001, Serpentinization and magmatism during extension at non-volcanic margins: the effect of initial lithospheric structure: Geological Society, London, Special Publications, v. 187, p. 551–576, doi:10.1144/GSL.SP.2001.187.01.27.

Peron-Pinvidic, G., Manatschal, G., and Osmundsen, P.T., 2013, Structural comparison of archetypal Atlantic rifted margins: A review of observations and concepts: Marine and Petroleum Geology, v. 43, p. 21–47, doi:10.1016/j.marpetgeo.2013.02.002.

Peron-Pinvidic, G., and Osmundsen, P.T., 2016, Architecture of the distal and outer domains of the Mid-Norwegian rifted margin: Insights from the Rån-Gjallar ridges system: Marine and Petroleum Geology, v. 77, p. 280–299, doi:10.1016/j.marpetgeo.2016.06.014.

Peron-Pinvidic, G., Osmundsen, P.T., and Ebbing, J., 2016, Mismatch of geophysical datasets in distal rifted margin studies: Terra Nova, v. 28, p. 340–347, doi:10.1111/ter.12226.

Picazo, S., Müntener, O., Manatschal, G., Bauville, A., Karner, G., and Johnson, C., 2016, Mapping the nature of mantle domains in Western and Central Europe based on clinopyroxene and spinel chemistry: Evidence for mantle modification during an extensional cycle: Lithos, v. 266–267, p. 233–263, doi:10.1016/j.lithos.2016.08.029.

Piccardo, G.B., Zanetti, A., and Müntener, O., 2007, Melt/peridotite interaction in the Southern Lanzo peridotite: Field, textural and geochemical evidence: Lithos, v. 94, p. 181–209, doi:10.1016/j.lithos.2006.07.002.

Pickup, S.L.B., Whitmarsh, R.B., Fowler, C.M.R., and Reston, T.J., 1996, Insight into the nature of the ocean-continent transition off West Iberia from a deep multichannel seismic reflection profile: Geology, v. 24, p. 1079–1082, doi:10.1130/0091-7613(1996)024<1079:IITNOT>2.3.CO;2.

Ranero, C.R., and Pérez-Gussinyé, M., 2010, Sequential faulting explains the asymmetry and extension discrepancy of conjugate margins: Nature, v. 468, p. 294–299, doi:10.1038/nature09520.

Reston, T., 2007, Extension discrepancy at North Atlantic nonvolcanic rifted margins: Depth-dependent stretching or unrecognized faulting? Geology, v. 35, p. 367–370, doi:10.1130/G23213A.1.

Reston, T.J., 1996, The S reflector west of Galicia: the seismic signature of a detachment fault: Geophysical Journal International, v. 127, p. 230–244, doi:10.1111/j.1365-246X.1996.tb01547.x.

Reston, T.J., 2009, The structure, evolution and symmetry of the magma-poor rifted margins of the North and Central Atlantic: A synthesis: Tectonophysics, v. 468, p. 6–27, doi:10.1016/j.tecto.2008.09.002.

Reston, T.J., Leythaeuser, T., Booth-Rea, G., Sawyer, D., Klaeschen, D., and Long, C., 2007, Movement along a low-angle normal fault: The S reflector west of Spain: Geochemistry, Geophysics, Geosystems, v. 8, p. Q06002, doi:10.1029/2006GC001437.

Reston, T.J., and McDermott, K.G., 2011, Successive Detachment Faults and Mantle Unroofing at Magma-Poor Rifted Margins: Geology, v. 39, p. 1071–1074, doi:10.1130/G32428.1.

Reston, T.J., and Pérez-Gussinyé, M., 2007, Lithospheric extension from rifting to continental breakup at magma-poor margins: rheology, serpentinisation and symmetry: International Journal of Earth Sciences, v. 96, p. 1033–1046, doi:10.1007/s00531-006-0161-z.

Reston, T.J., and Ranero, C.R., 2011, The 3-D geometry of detachment faulting at mid-ocean ridges: Geochemistry, Geophysics, Geosystems, v. 12, p. Q0AG05, doi:10.1029/2011GC003666.

Ryan, M.P., 1993, Neutral buoyancy and the structure of mid-ocean ridge magma reservoirs: Journal of Geophysical Research: Solid Earth, v. 98, p. 22321–22338, doi:10.1029/93JB02394.

Sanfilippo, A., and Tribuzio, R., 2011, Melt transport and deformation history in a nonvolcanic ophiolitic section, northern Apennines, Italy: Implications for crustal accretion at slow spreading settings: Geochemistry, Geophysics, Geosystems, v. 12, p. n/a-n/a.

Sauter, D. et al., 2013, Continuous exhumation of mantle-derived rocks at the Southwest Indian Ridge for 11 million years: Nature Geoscience, v. 6, p. 314–320, doi:10.1038/ngeo1771.

Sauter, D., Tugend, J., Gillard, M., Nirrengarten, M., Autin, J., Manatschal, G., Cannat, M., Leroy, S., and Schaming, M., 2018, Oceanic basement roughness alongside magma-poor rifted margins: insight into initial seafloor spreading: Geophysical Journal International, v. 212, p. 900–915, doi:10.1093/gji/ggx439.

Sawyer, D.S., Whitmarsh, R.B., and Klaus, A., 1994, Proceedings of the Ocean Drilling Program, Initial Reports, v. 149, doi:doi:10.2973/odp.proc.ir.149.1994.

Sayers, J., Symonds, P.A., Direen, N.G., and Bernardel, G., 2001, Nature of the continent-ocean transition on the non-volcanic rifted margin of the central Great Australian Bight: Geological Society, London, Special Publications, v. 187, p. 51–76, doi:10.1144/GSL.SP.2001.187.01.04.

Schuba, C.N., Gray, G.G., Morgan, J.K., Sawyer, D.S., Shillington, D.J., Reston, T.J., Bull, J.M., and Jordan, B.E., 2018, A low-angle detachment fault revealed: Three-dimensional images of the S-reflector fault zone along the Galicia passive margin: Earth and Planetary Science Letters, v. 492, p. 232–238, doi:10.1016/j.epsl.2018.04.012.

Sibuet, J.-C., 1992, New constraints on the formation of the non-volcanic continental Galicia–Flemish Cap conjugate margins: Journal of the Geological Society, v. 149, p. 829–840, doi:10.1144/gsjgs.149.5.0829.

Sibuet, J.-C., and Tucholke, B.E., 2012, The geodynamic province of transitional lithosphere adjacent to magma-poor continental margins: Geological Society, London, Special Publications, v. 369, p. SP369.15, doi:10.1144/SP369.15.

Sparks, D.W., and Parmentier, E.M., 1994, The Generation and Migration of Partial Melt beneath Oceanic Spreading Centers, *in* Magmatic Systems, M. P. Ryan, International Geophysics Series, v. 57, p. 55–76.

Stagg, H.M.J., Colwel, J.B., Direen, N.G., O'Brien, P.E., Bernardel, G., Borissova, I., Brown, B.J., and Ishirara, T., 2004, Geology of the Continental Margin of Enderby and Mac. Robertson Lands, East Antarctica: Insights from a Regional Data Set: Marine Geophysical Researches, v. 25, p. 183–219, doi:10.1007/s11001-005-1316-1.

Stagg, H., and Schiwy, S., 2002, Marine geophysical surveys completed off Antarctica: AusGeo News 66, p. 18–19.

Thinon, I., Matias, L., Réhault, J.-P., Hirn, A., Fidalgo-González, L., and Avedik, F., 2003, Deep structure of the Armorican Basin (Bay of Biscay): a review of Norgasis seismic reflection and refraction data: Journal of the Geological Society of London, v. 160, p. 99–116, doi:10.1144/0016-764901-103.

Totterdell, J.M., Blevin, J.E., Struckmeyer, H.I.M., Bradshaw, B.E., Colwell, J.B., and Kennard, J.M., 2000, A new sequence framework for the Great Australian Bight: starting with a clean slate.: APPEA Journal, p. 95–117.

Tribuzio, R., Riccardi, M.P., and Ottolini, L., 1995, Trace element redistribution in high-temperature deformed gabbros from East Ligurian ophiolites (Northern Apennines, Italy): constraints on the origin of syndeformation fluids: Journal of Metamorphic Geology, v. 13, p. 367–377, doi:10.1111/j.1525-1314.1995.tb00226.x.

Tucholke, B.E., Sibuet, J.C., and Klaus, A., 2004, Proceedings of the Ocean Drilling Program, Initial Reports, Volume 210, *in* v. 210.

Tucholke, B.E., Sawyer, D.S., and Sibuet, J.-C., 2007, Breakup of the Newfoundland–Iberia rift: Geological Society, London, Special Publications, v. 282, p. 9–46, doi:10.1144/SP282.2.

Tucholke, B.E., Behn, M.D., Buck, W.R., and Lin, J., 2008, Role of melt supply in oceanic detachment faulting and formation of megamullions: Geology, v. 36, p. 455–458, doi:10.1130/G24639A.1.

Tugend, J., Gillard, M., Manatschal, G., Nirrengarten, M., Harkin, C., Epin, M.-E., Sauter, D., Autin, J., Kusznir, N., and McDermott, K., 2018, Reappraisal of the magma-rich versus magma-poor rifted margin archetypes: Geological Society, London, Special Publications, p. SP476.9, doi:10.1144/SP476.9.

Tugend, J., Manatschal, G., and Kusznir, N.J., 2015, Spatial and temporal evolution of hyperextended rift systems: Implication for the nature, kinematics, and timing of the Iberian-European plate boundary: Geology, v. 43, p. 15–18, doi:10.1130/G36072.1.

Tugend, J., Manatschal, G., Kusznir, N.J., Masini, E., Mohn, G., and Thinon, I., 2014, Formation and deformation of hyperextended rift systems: Insights from rift domain mapping in the Bay of Biscay-Pyrenees: Tectonics, v. 33, p. 2014TC003529, doi:10.1002/2014TC003529.

Ulmer, P., and Trommsdorf, V., 1999, Phase relations of hydrous mantle subducting to 300 km, *in* Fei, Y., Bertka, C., and Mysen eds., Mantle Petrology: Field observations and High Pressure Experimentation, The Geochemical Sociiety, Special Publication 6, p. 24.

Ulmer, P., and Trommsdorff, V., 1995, Serpentine Stability to Mantle Depths and Subduction-Related Magmatism: Science, v. 268, p. 858–861, doi:10.1126/science.268.5212.858.

Wernicke, B., 1981, Low-angle normal faults in the Basin and Range Province: nappe tectonics in an extending orogen: Nature, v. 291, p. 645–648, doi:10.1038/291645a0.

White, R.S., McKenzie, D., and O'Nions, R.K., 1992, Oceanic crustal thickness from seismic measurements and rare earth element inversions: Journal of Geophysical Research: Solid Earth, v. 97, p. 19683–19715, doi:10.1029/92JB01749.

Whitmarsh, R.B., Beslier, M.O., and Wallace, P.J., 1998, Proceedings of the Ocean Drilling Program, Leg 173: Proc. ODP, Init. Repts, v. 173, p. 7–23.

Whitmarsh, R.B., White, R.S., Horsefield, S.J., Sibuet, J.-C., Recq, M., and Louvel, V., 1996, The ocean-continent boundary off the western continental margin of Iberia: Crustal structure west of Galicia Bank: Journal of Geophysical Research: Solid Earth, v. 101, p. 28291–28314, doi:10.1029/96JB02579.

Williams, S.E., Whittaker, J.M., Halpin, J.A., and Müller, R.D., 2019, Australian-Antarctic breakup and seafloor spreading: Balancing geological and geophysical constraints: Earth-Science Reviews, v. 188, p. 41–58, doi:10.1016/j.earscirev.2018.10.011.